Dysfunctional Hippocampal-Prefrontal Connectivity without Neuronal Loss Underlies Psychotic-Like Behaviors Following Early-Life Seizure

Running head: HPC-PFC dysfunction and psychosis in epilepsy

Rafael Naime Ruggiero[1*], Danilo Benette Marques[1#], Matheus Teixeira Rossignoli[1#], Jana Batista De Ross[1], Tamiris Prizon[1], Ikaro Jesus Silva Beraldo[2,3], Lezio Soares Bueno-Junior[4], Ludmyla Kandratavicius[5], Jose Eduardo Peixoto-Santos[6], Cleiton Lopes Aguiar[2,3], João Pereira Leite[1*].

[1]Department of Neuroscience and Behavioral Sciences, Ribeirão Preto Medical School, University of São Paulo, Ribeirão Preto, São Paulo, Brazil.
[2]Department of Physiology and Biophysics Federal University of Minas Gerais, Belo Horizonte, Minas Gerais, Brazil.
[3]Laboratory of Molecular and Behavioral Neuroscience (LANEC), Federal University of Minas Gerais, Belo Horizonte, Brazil
[4]Department of Psychiatry, University of Michigan Medical School, Ann Arbor, Michigan, USA
[5]Department of Pathology, State University of Campinas, Campinas, São Paulo, Brazil
[6]Neuroscience Discipline, Department of Neurology and Neurosurgery, Universidade Federal de São Paulo, São Paulo, Brazil

***Corresponding author:** rafaruggiero@gmail.com, jpleite@fmrp.usp.br
[#]DBM and MTR contributed equally to this work

Conflict of interest

The authors declare no competing financial interests.

Acknowledgements

This research was funded by Fundação de Amparo à Pesquisa do Estado de São Paulo - FAPESP (R.N.R.: 2018/02303-4; M.T.R.: 2020/01510-6; J.P.L.:

2016/17882-4), Coordenação de Aperfeiçoamento de Pessoal de Nível Superior - CAPES - Finance Code 001 (D.B.M.: 88882.328283/2019-01;), and Conselho Nacional de Desenvolvimento Científico e Tecnológico - CNPq (J.P.L.: 305104/2020-9 and 422911/2021-6; T.P.: 164165/2018-5). We thank Renato Meirelles e Silva, Renata Caldo Scandiuzzi and Daniela Ribeiro for technical support. We thank Ana Carolina Medeiros and Rafael D'Agosta for helping with the photomicrography and histology. We also thank Patrick Forcelli, Claudio Queiroz, Marcelo Caetano, Tonicarlo Velasco, Ricardo Saute and Norberto Garcia Cairasco for discussions. RNR and JPL designed the research. RNR, CLA and LSBJ developed the methodology. RNR, DBM, TP and MTR conducted the experiments. RNR, DBM, and IJSB analyzed data. MTR edited the figures. JBDR, LK, TP and JEPS performed immunohistochemistry. TP and JEPS conducted the neurochemistry experiments. JPL supervised the project. All authors wrote and revised the manuscript.

Abstract

Cognitive impairments and psychiatric symptoms affect up to half of patients with temporal lobe epilepsy and are often more detrimental to their quality of life than the seizures themselves. Evidence indicates that the neurobiology of epileptogenesis shares common pathophysiological mechanisms with psychiatric comorbidities. However, these mechanisms and how they relate to specific behavioral alterations are unclear. We hypothesized that a dysfunctional communication between the hippocampus and the prefrontal cortex, as a consequence of epileptogenesis, would be linked to behavioral and cognitive symptoms observed in the comorbidities of temporal lobe epilepsy. Here, we performed a multilevel study to investigate behavioral, electrophysiological, histopathological, and neurochemical long-term consequences of early-life *Status Epilepticus* in male rats. We found that adult animals submitted to early-life seizure (ELS) presented behavioral alterations typically found in animal models of psychosis, such as working memory deficits, hyperlocomotion, reduction in sensorimotor gating, and sensitivity to psychostimulants. Surprisingly, cognitive deficits were linked to an aberrant increase in hippocampus-prefrontal cortex (HPC-PFC) long-term potentiation (LTP) while sensorimotor alterations were associated with increased neuroinflammation, as

verified by glial fibrillary acidic protein (GFAP) expression, and altered dopamine neurotransmission. Noteworthy, ELS rats did not exhibit neuronal loss. Furthermore, ELS rats displayed impaired HPC-PFC theta-gamma coordination and an abnormal brain state during active behavior oddly similar to rapid eye movement (REM) sleep oscillatory dynamics. Our results point to impaired HPC-PFC functional connectivity as a possible pathophysiological mechanism by which an epileptogenic insult can cause cognitive deficits and psychosis-related manifestations even without structural damage, bearing translational implications for understanding and monitoring psychiatric comorbidities in epilepsy.

Introduction

Psychiatric disorders affect up to half of the patients with epilepsy and significantly impact their quality of life (Salpekar and Mula, 2019). Understanding the neurobiological mechanisms of these comorbidities is crucial to develop better treatments for patients with epilepsy. It is currently speculated that the neurobiology of epileptogenesis shares common pathophysiological mechanisms with non-ictal symptoms, especially cognitive and psychiatric symptoms (Jensen, 2011). Temporal lobe epilepsy (TLE) is the most prevalent type of acquired epilepsy and presents a higher incidence of psychiatric comorbidities than the general population and other extratemporal epilepsies (Dalmagro et al., 2012). Patients with TLE frequently have a history of *Status Epilepticus* (SE) during infancy, which is seen as an initial injury that triggers epileptogenic processes (Mathern et al., 2002).

Experimental studies indicate that early-life seizures (ELS) induce long-term cognitive and behavioral alterations with translational validity for the psychiatric manifestations observed in clinical epilepsies (Holmes, 2016). However, unlike clinical or experimental TLE, ELS models are not associated with severe neuronal loss (Baram et al., 2002). One possible mechanism is that ELS could have functional and molecular effects at the brain circuit level, producing relevant cognitive impairments (Kandratavicius et al., 2012b, 2012a). The hippocampus (HPC) is a fundamental brain region affected by ELS and TLE. HPC interaction with the prefrontal cortex (PFC) underlies cognitive processes and is impaired in neuropsychiatric disorders such as schizophrenia (Ruggiero et al., 2021). Impairments of HPC-PFC oscillatory dynamics are observed in genetic,

102 developmental, and pharmacological models of schizophrenia and are thought to
103 be essential to produce psychotic-like behavior (Sigurdsson and Duvarci, 2016).
104 Although it is well recognized that PFC and HPC are important for
105 neuropsychiatric disorders, little is known about how their neuronal dynamics are
106 affected by ELS. Here, we hypothesized that ELS would produce long-term
107 alterations in HPC-PFC neuronal dynamics related to cognitive deficits and
108 behavioral abnormalities (Ruggiero et al., 2012). To test this hypothesis, we
109 induced SE as a form of prolonged ELS and performed behavioral tests to assess
110 cognitive processes and psychotic-like behaviors. Then, we performed
111 neurophysiological, immunohistochemical, and neurochemical experiments to
112 study potential changes in the HPC-PFC circuits that could underlie such
113 behavioral alterations. We found that adult ELS rats present a myriad of
114 behavioral impairments that are typically observed in animal models of psychosis
115 and schizophrenia: working memory deficits, hyperlocomotion, sensorimotor
116 gating impairment, and behavioral sensitivity to psychostimulants. Remarkably,
117 we found an enhanced long-term potentiation (LTP) in the HPC-PFC pathway of
118 ELS animals, which was strongly associated with cognitive impairment. Our
119 results also describe neuroinflammation and alterations in dopaminergic
120 neurotransmission as major contributors to psychotic-relevant behavior. Freely-
121 moving experiments allowed us to observe HPC-PFC dynamics during different
122 brain states. ELS rats displayed an increased HPC theta and impaired
123 coordination of PFC gamma activity during active behavior. During rapid eye
124 movement (REM) sleep, ELS rats showed a reduction in HPC-PFC connectivity.
125 Notably, ELS rats presented an aberrant brain state during active behavior
126 characterized by oscillatory dynamics similar to REM sleep. Finally, we
127 implemented a linear discriminative model, which demonstrated that collective
128 patterns of oscillatory alterations accurately distinguished ELS from control
129 animals. Therefore, we identified a convergence of dysfunctional patterns at
130 multiple levels linking epileptogenesis and psychotic-like behaviors. These
131 convergent patterns indicate that epileptogenic processes triggered during early
132 life, such as neuroinflammation, could lead to altered neurotransmission and
133 consequently aberrant dynamics in the HPC-PFC coordination, potentially
134 contributing to the psychiatric comorbidities of epilepsy.
135

Materials and Methods

Animals

Wistar rats were housed in a colony room with controlled temperature (22 ± 2 °C) and a 12-h light/dark cycle with free access to food and water. Litters contained up to 8 animals with a maximum of 5 males. Rats were weaned at 21 days postnatally (P21). All procedures were performed according to the National Council for the Control of Animal Experimentation guidelines for animal research and approved by the local Committee on Ethics in the Use of Animals (Ribeirão Preto Medical School, University of São Paulo; protocol: 159/2014).

Experimental Designs

We used four cohorts (a total of 17 litters) to compare the effects of early-life *Status Epilepticus* (ELS) *versus* control (CTRL) animals. The first cohort was used for acute electrophysiology during the induction of ELS (n=5, ELS only). The second was used for behavioral tests (CTRL n=11, and ELS n=14), synaptic plasticity experiments (CTRL n=7, and ELS n=7), and immunohistochemistry (CTRL n=9, and ELS n=11). The third was used to investigate HPC-PFC dynamics in freely moving rats (CTRL n=6, and ELS n=9). Finally, in the fourth cohort, we assessed behavioral sensitization to psychostimulants (CTRL n=15, and ELS n=14) and neurochemical quantification (CTRL n=8, and ELS n=9).

Early-Life Status Epilepticus

At P11-P12 we induced a 2-hour SE using lithium chloride (LiCl, 127 mg/kg, i.p., Sigma-Aldrich, USA) 18-20 prior to injection of methylscopolamine (1 mg/kg, i.p., Sigma-Aldrich) and pilocarpine (80 mg/kg, s.c., Sigma-Aldrich, USA) (Kubová and Mareš, 2013). Behavioral seizures were monitored following the Racine scale (Racine, 1971). SE was interrupted by diazepam (5 mg/kg, i.p., Teuto, Brazil) at the 2-hour mark. During the recovery period (1 week post-ELS) we provided food supplementation and subcutaneous rehydration with saline and monitored body temperature and weight.

Behavior

The radial-arm maze working memory task was based on Floresco et al. (1997). Briefly, rats were kept at 85-90% of their initial body weight throughout

the 21 days of the experiment. Training consisted of single daily sessions, each one divided into the training phase and test phase, 30 min apart. During the training session, four doors were kept open providing access to food pellets. In the test session, all doors remained open, but with pellets available only in the four arms that were closed in the previous training session. The sessions were terminated upon full pellet consumption or after 5 min. Two types of errors were quantified: Reference error: reentering arms previously visited during the training session; Working memory error: reentering an arm already visited during the test session. The sum of both categories denoted the total errors for each animal.

Three days after returning to *ad libitum* diet, locomotor activity was evaluated for 30 min in the open field test (Wolf et al., 2016).

Immediately after the open field test, rats were examined for prepulse inhibition (PPI) of the acoustic startle. The PPI test consisted of a habituation period (5 min) followed by 72 trials (intertrial interval: 15 ± 8 s) with prepulse alone (PP), startling pulse alone (P), prepulse followed by a startling pulse (PP + P), and no stimulus, all of which accompanied by background noise (65 dB white noise). Startle-eliciting stimuli were presented at 120 dB for 40 ms (P) and prepulse stimuli were presented for 20 ms (PP, 1000 Hz; 71, 77, and 83 dB; 20 ms). Trials were presented in a random order, with each trial type being presented six times. We used the equation: %PPI = 100 − 100 × (mean startle amplitude at PP + P)/(mean startle amplitude at P) (Wolf et al., 2016).

In order to measure the effects of ELS on sensitization to psychostimulants, we performed the apomorphine-induced locomotion test. At P80-90, rats were placed in the open field apparatus and were allowed to roam for 60 min. Then, we injected apomorphine (APO, 1.5 mg/kg, i.p., Sigma-Aldrich, USA) and measured locomotion for another 60 min. The distance across blocks was normalized by Z-score to the mean of baseline blocks.

Synaptic Plasticity

199 HPC-PFC synaptic plasticity studies were performed as described in
200 previous works from our group (Bueno-Junior et al., 2018; Ruggiero et al., 2018).
201 Briefly, rats were anesthetized with urethane (1.2 mg/Kg in NaCl 0.15 M, i.p.) for
202 electrode implantation. A recording electrode (Teflon-coated tungsten wires 60
203 μm, AM-Systems) was inserted in the medial PFC (prelimbic region (PL), anterior-
204 posterior: 3.0 mm; medial-lateral, ML: 0.5 mm; dorsal-ventral, DV: 3.2 mm), and
205 a bipolar stimulation electrode (twisted wires; ~500 μm inter-pole distance) was
206 inserted in the ipsilateral HPC (intermediate CA1 AP: −5.6 mm; ML: 4.5 mm; DV:
207 2.5 mm). An additional burr hole was drilled over the right parietal cortex for a
208 reference screw. Temperature was kept constant at 37 ± 0.5°C during the
209 experiment.

210 HPC was stimulated with single monophasic pulses (200 μs, 0.05 Hz,
211 150–300 μA, 80-ms inter-pulse interval) while recording PFC field postsynaptic
212 potentials (fPSPs). Stimulation intensity (60–500 μA) was calibrated to evoke 50–
213 60% of the maximal fPSP amplitude. Field recordings were conditioned through
214 a preamplifier (100× gain, 0.03–3 kHz bandpass; Grass) and digitized at 10 kHz
215 (ADInstruments). For LTP induction, we used a high-frequency stimulation (HFS)
216 protocol consisting of 2 series (10 min apart) of 10 trains (0.1 Hz), each train with
217 50 pulses at 250 Hz (Ruggiero et al., 2018). fPSP amplitudes and slopes were
218 computed as the difference and slope between the positive and negative peaks,
219 respectively. Short-term synaptic plasticity was estimated by paired-pulse
220 facilitation (PPF), calculated as the ratio of the fPSP2 and fPSP1 (Lopes-Aguiar
221 et al., 2020). Amplitudes and slopes were normalized as ratios of the baseline
222 mean and averaged into 10-min bins.
223

224 ***Brain Tissue Processing***

225 *Immunohistochemistry*

226 We employed a standardized immunohistochemistry protocol (Peixoto-
227 Santos et al., 2015) to estimate NeuN+ neuronal density and to evaluate
228 parvalbumin-expressing (PV) interneurons, mGluR5 expression, and glial
229 fibrillary acid protein (GFAP) reaction. Briefly, endogenous peroxidases were
230 blocked and the antigens were exposed by microwave-induced retrieval. We
231 used the primary antibodies against NeuN (Chemicon, USA; 1:1000), PV
232 (Calbiochem, USA; 1:500), mGluR5 (Millipore, USA; 1:200), and GFAP (Dako,
233 Denmark; 1:500) proteins, and biotinylated secondary antibodies (Dako,
234 Denmark; 1:200). Revelation was performed with Elite ABC Kit (Vector) and
235 diaminobenzidine solution (Pierce).
236 Images from the regions of interest were captured at 200× magnification
237 in the Axio Scope.A1 microscope system (Carl Zeiss). The regions of interest
238 included the hippocampus (CA1 and GL, granule layer of dentate gyrus),
239 entorhinal cortex (EC), infralimbic (IL) and prelimbic cortex (PL), and thalamic
240 reticular nucleus (TRN). Images were then processed in Image J software (NIH,
241 USA; 1.48v). Data are shown as the density of NeuN positive cells and
242 immunopositive area for PV, mGluR5, and GFAP.
243
244 *High-Performance Liquid Chromatography (HPLC)*
245 Samples were taken bilaterally from the nucleus accumbens (NAc), PFC,
246 and HPC. The samples were homogenized with ultrasound in a 0.1 mol/L $HClO_4$
247 0.02% $Na_2S_2O_2$ solution containing dihydroxybenzylamine (DHBA, 146.5 ng/mL),
248 and homoserine (HSER, 10 µg/mL) as internal standards and at a dilution of 15
249 µL per sample milligram. We employed Shimadzu LC-10AD isocratic systems
250 with a fluorescence detector for glutamate (Glu) and gamma-aminobutyric acid
251 (GABA), and an electrochemical detector for dopamine (DA) and its metabolites
252 3,4-dihydroxyphenylacetic acid (DOPAC) as previously published (Castro-Neto
253 et al., 2013). The neurotransmitter levels were considered to reflect
254 neurotransmitter stock in synaptic vesicles, their metabolites reflected the
255 release, and metabolite/neurotransmitter ratios were taken as an index of
256 neurotransmitter turnover. Standards containing all amino acids and
257 monoamines/metabolites of interest were employed to define their respective
258 peaks in the samples.
259

260 ***Freely Moving Electrophysiology***

261 *Electrophysiological recordings*

262 Chronic head caps consisted of two eight-channel connectors (Omnetics),
263 one for the PFC (PL, 7 wires) and another for the HPC (intermediate CA1, 7 wires)
264 (Bueno-Junior et al., 2017; Marques et al., 2022). We additionally implanted a
265 recording wire into the trapezius muscle to serve as an electromyogram (EMG).
266 The EMG wire was soldered to the HPC connector. Microscrews were fastened
267 into the skull, including a ground reference in the intraparietal area. Animals were
268 allowed to recover for 8-9 days before recordings.

269 To record electrophysiological signals through sleep-wake states, rats
270 were placed into a shuttle box apparatus inside a soundproof box with food and
271 water *ad libitum*. Recordings varied between 30 to 48 hours, divided later into
272 periods of 6 hours for analysis. Local field potentials (LFP) were recorded through
273 a multichannel acquisition processor (Plexon) (1000× gain, 0.7-500 Hz bandpass
274 filter, 1-kHz sampling rate).

275

276 *Classification of sleep-wake states*

277 Classification of the sleep-wake cycle states was carried out through a
278 semi-supervised machine learning pipeline. The HPC theta (4.5-12 Hz), PFC
279 delta (0.7-4 Hz), and EMG (100-200 Hz) power were computed in 5-second
280 epochs without overlaps (4 tapers; time-bandwidth product: 2.5). A support vector
281 machine (SVM) (radial basis function) was trained to discriminate the epochs into:
282 (1) awake or sleep epochs using EMG power; (2) REM or NREM epochs based
283 on theta/delta ratio; (3) quiet wake (QWK) or active (ACT) epochs based on
284 theta/delta ratio. Later, we classified our recordings based on 30-second epochs
285 by grouping sets of six 5-second epochs and considering the most representative
286 state.

287

288 *Spike wave-discharge detection* (SWD)

289 For spike wave-discharge detection, we used the PFC recordings. First,
290 the short-time Fourier transform (STFT) was computed within 3-70 Hz throughout
291 250-ms windows with 50% overlap. A detection threshold was defined as the
292 mean + 1.5 standard deviation of the absolute value of the STFT of the frequency
293 bands 4.4-16.4, 17.6-32.8, and 35.1-55 Hz throughout the entire recording. SWD

events were detected when the average STFT of the aforementioned frequency bands at one epoch exceeded the threshold. Consecutive epochs above the threshold were grouped as the same event. The beginning and the end of an event were defined as the closest epochs when the average STFT was lower than the mean + 1 standard deviation of STFT of the frequency bands of interest. Lastly, the detected putative events were manually sorted by an expert.

Spectral estimates

We divided 30-s epochs into 3-s epochs for spectral analyses. Power spectrum densities (PSD) and magnitude-squared coherence were obtained using Welch's method with 1-s segments, 50% overlap, and Hamming windowing. Relative power was obtained by dividing values by the sum within 0.5-55 Hz for each epoch. We defined the frequency bands: delta (1-4 Hz), theta (4.5-11 Hz), low gamma (30-55 Hz), and high-gamma (65-100 Hz) to compare estimates and obtained the spectral peak of each epoch using MATLAB function *findpeaks*. We used the low and high-gamma peaks values to estimate a probability density function using kernel density estimate method (*kde* function in MATLAB) and compare ACT and REM state distributions.

To quantify theta oscillation power we used the FOOOF algorithm (Donoghue et al., 2020), which parametrizes the PSD separating the periodic and aperiodic components of the signal. We used frequencies within 3-40 Hz, the “fixed” aperiodic mode, a minimum peak height of 0.05, and a maximum number of peaks of 4 (https://fooof-tools.github.io/fooof/). EMG data were low-cut filtered (>30 Hz) and the sum of power within 30-200 Hz was obtained.

As a synchrony measure, we also computed cross-correlations between each pair of LFPs (low-pass filter of 50 Hz) recorded from the HPC and PFC using a maximum lag of 1 s. Coefficients were normalized so that the autocorrelations at zero lag were one. We observed that the highest coefficients occurred in the range of -80 to -20 ms (HPC leading the PFC), so we obtained the maximum coefficient within this range for each rat average for comparisons. Cross-spectrum power was calculated using Welch's method for the normalized correlation coefficients from -1 to 1 s.

For cross-frequency amplitude spectrum correlations, we computed the absolute STFT for each 3-s epoch throughout 100-ms segments with 50%

overlap and Hamming windowing across 0.5-Hz frequency bins within 0.5-200 Hz. We calculated the correlation matrix for each frequency pair using Pearson's R.

State maps

After state classification and spectral analysis, we computed two-dimensional state maps to investigate the natural distinction between sleep-wake states. The state maps were computed according to Gervasoni et al. (2004) and Dzirasa et al. (2006). First, we obtained the power *ratio 1* (4.5-9/4.5-50 Hz) and *ratio 2* (2-20/2-50 Hz) for each region and the first principal component, estimated by singular value decomposition algorithm considering both regions, for each ratio. Finally, we applied a Hann window of 10 epochs on scores throughout time for smoothing.

To identify the intermediate states (IS), we first estimated the trajectory *speed* of epochs throughout state map dimensions as the Euclidean distance between each epoch and its predecessor. Then, we defined a threshold of 0.1 and labeled the epochs with greater speed as IS. This threshold was determined heuristically, corresponding closely to the expected value plus a standard deviation from a Poisson distribution across rats.

From visual inspection and the literature (Gervasoni et al., 2004; Dzirasa et al., 2006), the state maps usually separate three well-defined clusters heuristically corresponding to awake, REM, and NREM sleep. To assure the correspondence between state map clusters and the classification outcomes, we performed Gaussian mixture models clustering of the state maps for 3 clusters and 80% posterior probabilities and computed Chi-squared tests with the classified NREM, REM, and awake (QWK+ACT) labels. Three animals were excluded for having outlier lower Chi-values. Although QWK and ACT states are often evenly distributed inside the awake cluster, QWK epochs may overlap with intermediate states closer to NREM, so the ACT epochs were considered to represent more precisely the localization of neural dynamics associated with behavior in the state map. The dissimilarity between ACT and REM states was estimated by the average pairwise state map Euclidean distance of all epochs between the two states.

We used machine learning algorithms to decode sleep-wake states from the state map. We used the ACT and REM state map *ratios 1* and *2* values. We applied a linear and radial basis function SVM *fictcsvm* function in MATLAB ('KernelFunction', 'linear' or 'rbf') as well as a Random Forest algorithm using the *fitcensemble* function in MATLAB ('Method', 'bag', 'NumLearningCycles', 50, for Random Forest) to decode states. We used the ACT and REM epochs from all the rats creating one single model for the CTRL or ELS condition. Using the same approach, we also constructed a random forest decoder model with non-reduced variables using 1 to 55 Hz (0.5 Hz bins) for the PFC and HPC power and coherence. Discrimination was evaluated using the area under the receiver operating characteristic curve (AUC-ROC). The point-wise confidence interval was calculated using a 1000-repetition bootstrap. Average AUC-ROC values were calculated using the prediction of the trained model on 20% of the epochs as test data and repeating the process 100 times.

Statistical Analysis

Data were analyzed using GraphPad Prism Software version 9.00 (GraphPad Software, LLC), and R studio version 2021. We used paired Student *t*-tests for within-group comparisons and two-sample *t*-tests for between-group comparisons. Two-way ANOVA with repeated measures (RM) was performed for comparisons across time bins, using Sidak's multiple comparison test as a *post-hoc*. To examine linear model assumptions, we analyzed the distribution of the residuals using a Q-Q plot, the Kolmogorov-Smirnov test, homoscedasticity, and the residual plot. We used the Mann-Whitney test to compare two groups and the Wilcoxon signed-rank test to paired comparisons as non-parametric alternatives. We calculated Pearson's linear correlation and Spearman's rank correlation as a nonparametric equivalent. To compare correlation and spectral coherence estimates we applied Fisher's Z transform to the data. For multiple comparisons in the neurochemical quantification, we performed Holm's procedure for multiple comparisons correction across neurotransmitters and metabolites per region.

Data are expressed as the mean ± SEM. The significance level was set to 0.05 unless stated otherwise. For some multiple comparisons, statistical values are expressed as the range. Significances are expressed as $^{\dagger}p < 0.1$, $^{*}p < 0.05$, $^{**}p < 0.01$, and $^{***}p < 0.001$.

Linear mixed-effects models

We also constructed statistical inferential models across time controlling for individual variability and litter using linear mixed-effects models. We compared power and coherence estimates throughout time by dividing the electrophysiological recording into 5 periods (6 hours). Group and time (periods) were assigned as fixed effects and subject, litter, and time were assigned as random effects. We used this approach to construct a maximal random effects structure model as preconized in the literature as more generalizable (Barr et al., 2013). The model was estimated by restricted maximum likelihood using the *lme* function of the *nlme* package (Pinheiro et al., 2023) with an unstructured covariance matrix.

Multivariate analysis

Each variable was Z-scored before multivariate analysis. We constructed correlograms to assess the relationship within behavioral and neurobiological measures. Variables were sorted by agglomerative hierarchical clustering using Ward's method and correlation as the metric. We also performed agglomerative hierarchical clustering of subjects using Ward's method and Euclidean distance as the metric to assess how unsupervised clustering by our multivariate data might match the experimental groups. An optimal number of clusters was estimated using the silhouette method and final definition was based on parsimonious interpretability of the results.

Principal component analysis (PCA), using singular-value decomposition, was used for dimensionality reduction to find collective patterns of variance within behavioral variables (behavior factors) and neurobiological variables (neurobiology factors), and to reduce each immunohistochemical measure across all brain regions into single scores. Principal components (PCs) were projected onto data and the mean score was compared between conditions.

Canonical correlation analysis (CCA) was performed to describe multivariate relationships between behavioral and neurobiological measures. Missing data were imputed using the multiple imputation by chained equations algorithm. For CCA, we used the first PC (PC1) and second PC (PC2) of behavioral variables as inputs for the behavioral factors and the PC1 of each

429 immunohistochemical variable (NeuN, PV, mGluR5, and GFAP,) across all brain
430 regions and the Z-scored LTP data as inputs for the neurobiological factors.
431 Variables were narrowed down from 30 to 7, which is statistically appropriate for
432 our sample size. We used the CCA package in R to obtain the canonical
433 dimensions and performed the Hotelling-Lawley trace statistic to assess the
434 significance of each dimension.

435 We used multivariate generalized linear models (GLM) with a Gaussian
436 family and an identity link function. Quasi-Poisson regression (quasi-Poisson
437 family and logarithmic link function) were used for count data with overdispersion
438 (Errors in the radial maze) using a quadratic covariate (LTP). We constructed two
439 types of models: 1) a full model considering all the covariates; and 2) a restricted
440 model using backward stepwise model selection based on the Akaike information
441 criterion.

442 To assess the effectiveness of neurophysiological features in
443 discriminating CTRL from ELS rats, we fitted a regularized linear discriminant
444 classifier model on the PCA scores of selected electrophysiological variables. We
445 used the MATLAB function *fitcdiscr* without hyperparameter optimization. The
446 linear classifier using two predictors allowed the graphical representation and
447 avoided the overfitting of a high number of variables. Accuracy was determined
448 as the probability of correct category assignments using leave-one-out cross-
449 validation. We also determined the contribution of each original
450 neurophysiological variable by assessing their respective AUCs using a
451 univariate logistic regression model.

452

453 **Results**

454 **ELS induces a psychotic-like behavioral phenotype**

455 SE induced by lithium-pilocarpine in early life (Fig. 1A) produced an
456 unequivocal and stereotyped seizure, consisting mainly of forelimb myoclonus
457 and orofacial automatism (Racine 3), with some animals showing further
458 development into bilateral forelimb myoclonus, rearing and falling (Racine 4 and
459 5)(Racine, 1971). Seizures were confirmed electrophysiologically in freely
460 moving recordings of the frontal cortex and HPC, with paroxysms starting 10 min
461 after pilocarpine injection and persisting for at least 120 min (Fig. 1B).

462 Next, we investigated the long-term behavioral consequences of ELS (Fig.
463 2A). First, we evaluated possible weight differences as a confounder of
464 behavioral measures. ELS rats displayed weight loss on the day after SE (Two-
465 way RM ANOVA, treatment effect: $F_{(9,207)} = 11.7$, $p < 0.0001$, Sidak's *post-*
466 *hoc:* $p < 0.0001$; Fig. 2B). However, ELS animals recovered the pace of normal
467 weight gain in the subsequent days (*post-hoc*: $p > 0.05$) and into adulthood (Fig.
468 2C), showing no distinction to CTRL before (*t*-test, $t_{(23)} = 1.440$, $p = 0.1634$) or
469 during food restriction (*t*-test,$t_{(23)} = 0.0535$, $p = 0.9577$), indicating that behavioral
470 effects were unrelated to weight differences or alterations in food-seeking.
471 Importantly, when examined for spatial memory in the radial-arm maze,
472 ELS rats presented a specific increase in working memory errors (Mann-Whitney
473 test, $U = 36.5$, *n(CTRL, ELS)* = 11, 14, $p = 0.0254$; Fig. 2D). We found no
474 differences in the total reference errors (*t*-test, $t_{(23)} = 1.719$, $p = 0.0991$; Fig 2D)
475 and in the learning curve (Two-way RM ANOVA, treatment effect: $F_{(1,23)} =$
476 0.8032, $p = 0.3794$; Fig 2E). ELS rats presented significantly higher locomotion
477 in the open field test (Mann-Whitney test, $U = 27$, *n(CTRL, ELS)* = 11/14, $p =$
478 0.0051; Fig. 2F). ELS rats also presented a higher startle response (*t*-test, $t_{(23)} =$
479 2.757, $p = 0.011$; Fig. 2G) and a deficit in sensorimotor gating represented by a
480 reduction in PPI of the acoustic startle (Two-way RM ANOVA, treatment
481 effect: $F_{(2,46)} = 19.6$, $p < 0.0001$, Sidak's *post-hoc:* PPI 71 dB: $p = 0.0017$; PPI 77
482 dB: $p = 0.1040$; PPI 83 dB: $p = 0.030$; Fig. 2H).
483 Interestingly, all these behavioral alterations are typical of animal models
484 of psychosis (Sigurdsson, 2016). We investigated if collective patterns of
485 behavioral alterations induced by ELS could reflect latent factors representing
486 more comprising behavioral dimensions associated with psychosis. Working
487 memory errors in the radial-arm maze showed little correlation with the other
488 behavioral variables, while psychotic-like behaviors presented a strong
489 correlation with each other. PPI exhibited a positive correlation with every
490 intensity and a negative correlation with startle response and locomotion (Fig. 2I).
491 We also performed PCA to distinguish patterns of variance between multivariate
492 behavioral data (Fig. 2J-M). Our analysis indicated that dimensionality reduction
493 by PCA using the first two components explained 71.32% of the variability of the
494 data (Fig. 2J). By analyzing the loadings of the PC1, the variables that contribute
495 more strongly (>0.5) to this dimension were: high total distance, startle reflex, and

496 low PPI scores, indicating this component represents a latent factor of
497 sensorimotor dysfunction related to psychotic-like behaviors. In turn, the PC2
498 represents the cognitive dimension of the behavioral variables, as it presents a
499 high loading value (>0.5) for working memory errors (Fig. 2K). Finally, we found
500 that these PCs clearly distinguished CTRL from ELS animals, which presented
501 higher values of PC1 (PC1: *t*-test, $t_{(23)}$ = 3.9713, p = 0.0006; PC2: *t*-test, $t_{(23)}$ =
502 1.6466, p = 0.1132; Fig. 2L-M). These results indicate that the covariance across
503 behavioral tests can be summarized by a latent *psychotic factor* (PC1) and a
504 *cognitive factor* (PC2), representing two distinct dimensions of the behavioral
505 phenotype and suggesting possibly different neurobiological bases.
506
507 **Aberrant HPC-PFC synaptic plasticity in animals submitted to ELS**
508 Next, we tested the hypothesis that behavioral abnormalities in ELS rats
509 could be associated with synaptic plasticity impairments of the HPC-PFC
510 pathway (Fig. 3A-C). First, we looked for ELS-related alterations in basal synaptic
511 efficacy before inducing LTP. Synaptic efficacy was assessed in terms of basal
512 fPSP amplitude and slope (amplitude: *t*-test, $t_{(12)}$ = 1.278, p = 0.2255; slope: *t*-
513 test, $t_{(12)}$ = 0.5470, p = 0.5944; Fig. 3D), input-output curve (fPSP amplitude as a
514 function of stimulus intensity) (Two-way RM ANOVA, treatment effect: $F_{(1,12)}$ =
515 0.6596, p = 0.4325; Fig. 3E) and PPF curve (PPF as a function of the inter-pulse
516 interval) (Two-way RM ANOVA, treatment effect: $F_{(1,12)}$ = 0.3345, p = 0.5737;
517 Fig. 3F). None of these measures indicated alterations in ELS when compared to
518 CTRL (Fig. 3D-F).
519 Then, we proceeded to the actual synaptic plasticity experiments and
520 found that ELS rats presented an abnormally augmented LTP compared to CTRL
521 (Fig. 3G; Two-way RM ANOVA, treatment effect: $F_{(1,12)}$ = 7.54, p = 0.0177;
522 interaction effect: $F_{(26,312)}$ = 7.393, p < 0.0001; Sidak's *post-hoc:* p < 0.05 for 10-
523 60 min; *t*-test, $t_{(12)}$ = 2.747, p = 0.0177; Fig. 3G inset), despite the lack of
524 alterations in basal synaptic efficacy described above (Fig. 3D-F). Aberrant LTP
525 in the ELS rats was also observed when analyzing the fPSP slope (Two-way RM
526 ANOVA, treatment effect: $F_{(1,12)}$ = 4.757, p = 0.0498; interaction effect: $F_{(26,312)}$ =
527 4.120, p < 0.0001; Sidak's *post-hoc:* p < 0.05 for 10-40 min; Fig. 3H; *t*-test, $t_{(23)}$ =
528 2.794, p = 0.0162; Fig. 3H inset). However, short-term plasticity measured by
529 PPF decreased during the initial 30 min of recording (Two-way RM ANOVA,

530 interaction effect: $F_{(26,312)} = 3.457$, $p < 0.0001$; Sidak's *post-hoc:* $p < 0.05$ for 20-
531 30 min; Fig. 3I), possibly reflecting a ceiling effect on fPSP amplitude after LTP
532 induction. With these results, we demonstrate that, although ELS does not affect
533 basal synaptic efficiency, it significantly increases the ability of HPC-PFC circuits
534 to undergo LTP.
535
536 **ELS induces long-term neural inflammation, but not neuronal loss**
537 We sought to investigate histopathological alterations in cortico-limbic
538 circuits that could underlie the abnormalities in behavior and HPC-PFC synaptic
539 plasticity of ELS rats (Fig. 4A). Noteworthy, ELS rats did not present neuronal
540 loss when adults (Mixed-effects model, $F_{(1,12)} = 0.7683$, $p = 0.3980$; uncorrected
541 Mann-Whitney test, $p = 0.1666$-0.9372; Fig. 4B). Since neuronal loss is a
542 conspicuous finding related to cognitive deficits and behavioral alterations in
543 clinical and experimental TLE, our data show that cognitive impairments and
544 psychotic-like phenotypes can occur even without significant neuronal loss in the
545 HPC or PFC. Also, ELS did not produce long-term effects in the expression of PV
546 (Mixed-effects model, $F_{(1,13)} = 0.008$, $p = 0.9297$; uncorrected Mann-Whitney
547 test, $p = 0.3659$-0.9307; Fig. 4C) or mGluR5 receptors (Mixed-effects
548 model, $F_{(1,11)} = 0.0011$, $p = 0.9735$; uncorrected Mann-Whitney test, $p = 0.2467$-
549 0.8181; Fig. 4D). Finally, we found a strong increase in neuroinflammation,
550 verified by the marked expression of GFAP in ELS rats in all regions investigated
551 except the infralimbic cortex (Mixed-effects model, $F_{(1,18)} = 5.368$, $p = 0.0325$;
552 uncorrected Mann-Whitney test, $p = 0.0067$-0.0419 for GL, CA1, EC, PL, and
553 TRN, and $p = 0.2298$ for IL; Fig. 4E). These results show that ELS produces brain
554 inflammation later in life but without an evident neuronal loss.
555
556 **Cognitive impairment and psychotic-like behavior are distinctly correlated**
557 **with abnormal LTP and neuroinflammation**
558 By understanding the association between behavioral and neurobiological
559 variables, we would be able to infer putative mechanisms underlying the
560 behavioral comorbidities observed in ELS animals. To investigate multivariate
561 relationships between the behavioral (cognitive and psychotic factors) and
562 neurobiological (synaptic plasticity and immunohistochemical measures)
563 dimensions of ELS effects, we conducted CCA (Fig. 5A). CCA produced a

564 significant high-correlation model ($r = 0.94$, Hotteling-Lawley trace test, *F-*
565 *approximation*$_{(10,12)} = 3.2311$, $p = 0.0164$; Fig. 5B) that clearly separated CTRL
566 from ELS (behavior canonical dimension, *t*-test, $t_{(11)} = 3.693$, $p = 0.0035$;
567 neurobiology canonical dimension, *t*-test, $t_{(11)} = 3.917$, $p = 0.0024$; Fig. 5C). By
568 analyzing the coefficients, we observed that the behavior canonical dimension
569 showed higher values for the psychotic factor, but also included the cognitive
570 factor, although at a lower degree (Fig. 5D). The neurobiology canonical
571 dimension showed a larger value for the GFAP, intermediate values for LTP and
572 PV and the lowest coefficients for NeuN and mGluR5 (Fig. 5D). A similar pattern
573 was observed when analyzing the loadings for each dimension (Fig 5E). Notably,
574 the neurobiological variables have only weak correlations between them (Fig.
575 5F). To further dissect specific multivariate relationships between behavioral and
576 neurobiological measures, we constructed generalized linear models (GLM). The
577 GLM indicates GFAP, PV, and LTP as the most significant variables that explain
578 the psychotic factor variance (coefficients = 2.3775, 0.8457, and 0.5187; p =
579 0.1164, 0.00548, 0.08474 for GFAP, PV, and LTP, respectively, (Fig. 5G).
580 Accordingly, GLM multivariate regression indicates a strong association between
581 the psychotic factor and all significant GLM coefficients (GFAP + PV + LTP: r^2 =
582 0.7974, $p = 0.0116$; Fig. 5H), as well as psychotic factor and univariate
583 neurobiological measures (GFAP: $r = 0.6840$, $p = 0.0099$; Fig. 5I, PV: $r = 0.6548$,
584 $p = 0.0151$; Fig. 5J). Strikingly, we found a quadratic relationship between
585 synaptic plasticity effects and cognitive impairment. Poor performance on the
586 working memory test was observed in rats that presented too low or too high
587 values of HPC-PFC LTP, suggesting a U-shaped relationship between LTP and
588 cognitive performance (Fig. 5K-L). We observed this quadratic relationship using
589 both the cognitive factor (gaussian GLM, LTP coefficient = 1.22, $p = 0.0162$; Fig.
590 5 K) and raw error values from the radial maze test using a quasi-Poisson GLM
591 ($p = 0.00843$; Fig. 5L).
592 Taken together, both neuroinflammation and synaptic plasticity alterations
593 may underlie the behavioral effects of ELS, with neuroinflammation being more
594 associated with the psychotic-like dimension and LTP with the cognitive
595 dimension.
596
597 **ELS animals present epileptiform-like activity when adults**

598 Given the results above, we decided to further investigate the relationships
599 between circuit dynamics and behavioral dysfunctions during different brain
600 states using chronic electrophysiology recordings. We classified LFP epochs into
601 active wake (ACT), non-REM (NREM) sleep, rapid eye movement sleep (REM),
602 and quiet wake (QWK; Fig. 6A-D). No CTRL *vs.* ELS differences were found in
603 sleep architecture, according to the mean consecutive duration of each state,
604 percentage of time awake, number of persistent episodes in each state (Two-way
605 RM ANOVA, $F_{(1,13)} = 0.6500$, $p > 0.4346$; Fig. 6E-G), and percentage of time in
606 each state (Two-way RM ANOVA, $F_{(1,13)} = 0.5425$, $p > 0.4745$; Fig. 6H).

607 We also examined if ELS animals presented ictal activity during
608 recordings. We found that 44.45% of the ELS animals presented electrographic
609 discharges similar to spike-wave discharges (SWD) or rhythmical spiking (Fig.
610 6H-I). SWDs occurred mainly during NREM sleep and less often in QWK and
611 ACT but rarely occurred during REM epochs (Fig 6J-L). The SWDs were not
612 found in the CTRL rats, indicating that ELS induces an epileptogenic process.
613

614 **Increased HPC theta power during behavioral activity in ELS animals**

615 We initially concentrated our investigation on the ACT behavioral state to
616 associate oscillatory patterns with the behavioral abnormalities observed. We
617 found that ELS animals presented a higher theta power during ACT states in the
618 HPC (*t*-test, $t_{(13)} = 2.259$, $p = 0.0417$; Fig. 7A-D), but not in the PFC (*t*-test, $t_{(13)} =$
619 0.2636, $p = 0.7961$; Fig. 7B). This increased theta activity is more prominent
620 during the first periods of recording and exploration of the new environment
621 (linear mixed-effects model, $t = 2.10$, $p = 0.055$; Uncorrected *t*-tests for period
622 comparison: $t_{(13)} = 2.145$, 2.367, and 2.319, $p = 0.051$, 0.034, and 0.037 for
623 periods 1, 2, and 3 respectively; Fig. 7E). To further explore whether theta power
624 increase reflects a true oscillation and is not due to alterations in the aperiodic
625 components of the PSD, we also performed a PSD parametrization to separate
626 the theta oscillation (Fig. 7F). We found an increase in the theta oscillatory activity
627 in ELS animals during ACT states, indicating an actual oscillatory effect (Mann-
628 Whitney, $U = 7$, $n = (6,9)$, $p = 0.0176$; Fig. 7G-H). Hippocampal theta is well
629 known to occur during periods of locomotor activity, e.g., postural changes, head
630 movements, and rearing (Buzsáki and Moser, 2013) representing a possible

confounder. To control for this, we co-examined HPC theta power and EMG distributions during active states in CTRL *vs.* ELS rats (Fig. 7I). Indeed, theta oscillatory increase in ELS animals did not appear to be related to more movement, as we did not observe a significant association between EMG and theta power. In contrast, we found higher theta power in ELS animals even at low levels of EMG activity (Fig. 7I).

ELS promotes abnormal gamma coordination in the PFC during behavioral activity

Given the well-documented PFC gamma alterations in animal models of psychosis (Sigurdsson, 2016), we investigated the possible effects of ELS on PFC gamma activity during active states. ELS animals showed a reduced theta-gamma amplitude correlation during ACT states (*t*-test, $t_{(13)} = 2.851$, $p = 0.0136$; Fig. 8A-C), indicating that high-gamma activity is less coordinated, despite the increase in theta power. Interestingly, there were no increases in both low or high-gamma power (low-gamma: Mann-Whitney, $U = 16$, $n = (6,9)$, $p = 0.2238$; high-gamma: Mann-Whitney, $U = 24$, $n = (6,9)$, $p = 0.7756$; Fig. 8D). Amplitude correlation is an indicator of large-scale cortical interactions that govern cognition (Siegel et al., 2012). Thus, the lower theta-high gamma correlations found here may be related to the cognitive disruptions caused by ELS.

Next, we found a reduction in the PFC spectral exponent in ELS animals accessed by aperiodic PFC activity during ACT state (Fig. 8E), distribution of the aperiodic component (exponent and offset, Fig 8.F), and comparison in exponent parameter between groups (*t*-test, $t_{(13)} = 2.010$, $p = 0.0656$; Fig. 8G). Reductions of the spectral exponent have been discussed to indicate increased excitation/inhibition imbalance (Gao et al., 2017). This abnormal gamma dynamics in the ELS indicates a less coordinated oscillatory activity, which may reflect impaired limbic-cortical or cortico-cortical interactions that underlie cognitive dysfunctions.

ELS impairs HPC-PFC coherence during REM sleep

HPC-PFC connectivity during REM sleep is essential for memory consolidation (Lesting et al., 2013). Because we found cognitive impairments in ELS animals, we investigated HPC-PFC interactions during REM. First, we

665 observed that the theta power in the PFC and HPC during REM is not different
666 between groups (PFC: *t*-test, $t_{(13)}$ = 1.320, p = 0.2096; HPC: *t*-test, $t_{(13)}$ =
667 0.3557, p = 0.7278; Fig. 9A-B). However, we found that ELS rats show reduced
668 HPC-PFC connectivity in the theta band, measured by spectral coherence during
669 REM sleep (*t*-test, $t_{(13)}$ = 2.183, p = 0.0480; Fig. 9C-D). This difference is present
670 throughout the entire recording, as observed by the comparisons for all 6-hour
671 periods (linear mixed-effects model, t = -2.27, p = 0.0408; Fig. 9D, right). We
672 further confirmed this difference by analyzing the cross-correlation and cross-
673 spectrum power of the HPC-PFC LFP during REM (Fig. 9E-G). Cross-correlation
674 analysis reveals a clear directionality between signals from the HPC to the PFC
675 in both groups that happens markedly at a specific lag (-80 to -20 ms; Fig. 9E), in
676 which ELS rats present the most profound decrease in the correlation peak (*t*-
677 test, $t_{(13)}$ = 2.533, p = 0.0250; Fig. 9F-G).
678 We noticed from inspecting the theta coherence changes between ACT
679 and REM – the two states with the strongest theta coherence – that all CTRL
680 animals exhibited greater theta coherence during REM (paired *t*-test, $t_{(5)}$ =
681 8.023, p = 0.0005; Fig. 9H), while in the ELS group, part of the animals did not
682 present such an increase (paired *t*-test, $t_{(8)}$ = 1.924, p = 0.09; Fig. 9H). This
683 dynamic is further illustrated by observing the coherence changes across REM,
684 QWK, and ACT states. While most CTRL rats present an inclined decrease from
685 REM to QWK and a slight increase from QWK to ACT, ELS rats display a flatter
686 curve (Fig. 9I). By quantifying the homogeneity of the distributions of average
687 theta coherence values across states with entropy, we found a significantly higher
688 entropy (more homogeneous) in ELS than CTRL (paired *t*-test, $t_{(13)}$ = 2.695, p =
689 0.0184; Fig. 9JI). These results indicate that ELS promotes impairment in HPC-
690 PFC connectivity during REM sleep and in the regulation of state-dependent
691 dynamics.
692
693 **ELS rats display REM-like oscillatory dynamics during active behavior**
694 After we noticed that ELS animals show less distinction of some
695 electrophysiological activities between states, particularly REM and ACT, we
696 decided to further characterize the long-term effects of ELS on HPC-PFC state-
697 dependent oscillatory dynamics across the sleep-wake cycle. For that, we
698 constructed a state map based on two spectral power ratios (Gervasoni et al.,

2004; Dzirasa et al., 2006). This state map framework allows consistent characterization of all major brain states, revealing a dynamic global structure produced by the collective activity of forebrain structures (Gervasoni et al., 2004). First, we verified that the state maps reflected other brain and muscle activities that were not directly used for the map construction, such as the concentrated distribution of the PFC delta power during NREM, of the HPC theta/delta ratios in REM, of the EMG power in awake states, and of HPC-PFC theta coherence in both REM and awake states (Fig. 10A). Thus, as expected, our state maps presented three distinct clusters that precisely located REM, NREM, and ACT epochs (Fig. 10B).

Using this approach, a previous study reported an overlap between awake and REM states in a mouse model of schizophrenia (Dzirasa et al., 2006). Because we found ELS-related functional changes specifically during ACT and REM, we sought to investigate the convergence between these two states. Remarkably, we also found that ELS rats showed a significant similarity between the REM and ACT states (Fig. 10B). While in CTRL rats the distributions of Euclidean distances were larger, homogeneous, and symmetrical (Fig. 10C), ELS rats presented highly variable patterns across animals, most of which with skewed distributions concentrated at shorter distances (Fig. 10C). Indeed, the Euclidean distance was significantly reduced in ELS (*t*-test, $t_{(13)} = 2.326$, $p = 0.0369$; Fig. 10D), suggesting that the spectral features of REM and ACT are more similar in ELS animals.

Interestingly, we observed that this difference in states similarity was stronger in the initial 12 hours of recording, which corresponds to the periods of habituation to the novel environment (*t*-test, for periods 1-2: $t_{(13)} = 2.45$, $p = 0.029$; for periods 3-4: $t_{(13)} = 0.9409$, $p = 0.3638$; Fig. 10E).

To further demonstrate the higher similarity between REM and ACT states in ELS animals, we used machine learning algorithms in an attempt to separate these brain states through a *brute-force* approach. We observed that the two algorithms tested had the worst discriminative performance in the ELS rats, as verified by the smaller AUC-ROC (*t*-test, for SVM: $t_{(198)} = 99.59$, $p < 0.0001$; for random forest: $t_{(198)} = 107.6$, $p < 0.0001$; Fig. 10F). This worse discriminative performance also arises when using random forest algorithm (which presents the best discriminative performance) on the original whole-spectrum high-

733 dimensional variables (*t*-test, for PFC power: $t_{(198)} = 21.34$, $p < 0.0001$; for HPC
734 power: $t_{(198)} = 58.78$, $p < 0.0001$; for coherence: $t_{(198)} = 80.82$, $p < 0.0001$; for all
735 the spectral estimates combined: $t_{(198)} = 39.23$, $p < 0.0001$; Fig. 10G). This lack
736 of discriminative performance once again corroborates spectral similarities
737 between REM and ACT states in ELS rats.
738
739 **ELS rats present behavioral and neurochemical sensitivity to dopaminergic**
740 **activation**
741 REM-like neural oscillations during the awake state were described in
742 pharmacological and genetic animal models of hyperdopaminergia (Dzirasa et
743 al., 2006). In this context, we conducted a final experiment to investigate the
744 susceptibility of ELS rats to dopaminergic activation using apomorphine
745 (unspecific dopaminergic agonist). We examined behavioral sensitivity by
746 comparing the locomotion produced by apomorphine in the open field (Fig. 11A).
747 Our data demonstrate that apomorphine produces a higher increase in
748 locomotion in ELS rats when compared to CTRL across time blocks (Two-way
749 RM ANOVA, treatment effect: $F_{(1,27)} = 4.260$, $p = 0.0487$, Sidak's *post-hoc:* 5
750 min $p = 0.0376$; Fig. 11B) or between average normalized distances (Mann-
751 Whitney, *n(CTRL, ELS)* = 14/15, $U = 32$, $p = 0.0009$; Fig. 11B inset).
752 Immediately after the behavioral test, we collected samples of NAc, PFC,
753 and HPC to quantify neurotransmitters. The NAc was included in this analysis
754 because it is highly implicated in dopamine sensitivity and exploratory behavior
755 (Gomes et al., 2020). Our data demonstrate that apomorphine reduces dopamine
756 in the NAc of ELS rats, with no effects on dopamine turnover, as measured by
757 DOPAC/DA ratio (Sidak's multiple correction procedure, $t_{(12)} = 3.656$, $p = 0.0033$;
758 Fig. 11C). Still, a GLM model implicated NAc dopamine turnover as a significant
759 predictor of apomorphine-induced hyperlocomotion (*coefficient* = -0.7108, $p =$
760 0.00297; Fig. 11D). Consistently, apomorphine is known to reduce endogenous
761 DA release and DA metabolism in rodents and humans (Ozaki et al., 1989; de La
762 Fuente-Fernández et al., 2001). We also observed a reduction in dopamine
763 turnover in the HPC of ELS rats (Sidak's multiple correction procedure, $U = 9$, $p =$
764 0.0164; Fig. 11E) but no significant effects in the PFC.
765 Interestingly, we found that the HPC of ELS rats shows a higher Glu
766 content and higher Glu/GABA ratio than CTRL animals following apomorphine

injection (Sidak's multiple correction procedure, Glu: $t_{(15)} = 2.566$, $p = 0.0215$; Glu/GABA: $U = 9$, $p = 0.0079$; Fig. 12F) indicating possible disturbances in the excitation/inhibition balance.

HPC-PFC oscillatory dynamics discriminate ELS individuals

After identifying the relevance of specific electrophysiological variables throughout the study, we sought to investigate if collective patterns of the electrophysiological covariates across individuals could assemble a multidimensional oscillatory signature that distinguishes the ELS subjects. Based on relevance, particularity, and state specificity, for this investigation, we chose: (1) HPC theta power (Fig. 7H), (2) theta coherence entropy (Fig. 9J), (3) PFC exponent (Fig. 8G), (4) PFC theta-gamma correlation (Fig. 8C), (5) theta coherence (Fig. 9D), and (6) state map distance (Fig. 10D). By performing PCA, we observed that the first two principal components completely discriminated ELS from CTRL animals (Fig. 12A). This discrimination was further confirmed by fitting a linear discriminant classifier (traces on Fig. 12A) that achieved a 100% accuracy using the entire dataset and 80% accuracy on leave-one-out cross-validation.

Furthermore, unsupervised clustering almost completely discriminated ELS from CTRL rats dividing all the animals into two major clusters: a predominantly ELS cluster (81.82% of ELS animals) and a complete CTRL cluster (100% of CTRL animals; Fig. 12B-C). This data demonstrates that the electrophysiological variables used here are jointly affected by ELS at the functional level. In addition, the hierarchical clustering approach evidenced a progression of ELS-related oscillatory alterations, with a subcluster presenting an overlap between ELS and CTRL but the other with a more pronounced abnormal spectral fingerprint (Fig. 12B). Finally, we show that all the single electrophysiological variables have a high discriminative value (AUC > 0.7) (Fig. 12D), yet, their multivariate linear combination represented by PC1 scores (Fig. 12A) has the best classification performance with an AUC of 1.

Discussion

Here we showed that ELS leads to long-term behavioral abnormalities that are well-established translational features of psychosis. Remarkably, these

behaviors occurred independently of neuronal loss. Instead, they correlated with neuronal inflammation, hypersensitive dopaminergic neurotransmission, and aberrant HPC-PFC synaptic plasticity. We also found that ELS rats exhibit brain state-dependent alterations – particularly during active behavior and REM sleep – characterized by increased theta power and impaired coordination of local and long-range activity. In addition, ELS presents an abnormal oscillatory state during active behavior oddly similar to REM sleep. Finally, the collective pattern of oscillatory alterations accurately distinguishes ELS from control animals.

Common pathophysiological mechanisms underlying epileptogenesis, psychosis, and cognitive impairments

Studies usually describe increased locomotion (Kubová and Mareš, 2013) and working memory deficits (Tsai et al., 2012) as consequences of ELS. In addition to confirming these findings, we also found reduced PPI, which is less studied, but also a well-established correlate of positive symptoms in clinical psychosis (Turetsky et al., 2007; Ziermans et al., 2011). Here, we presented a multivariate *behavioral factor* comprising phenotypes of psychosis frequently reported in pharmacological, genetic, and developmental models of schizophrenia (Ruggiero et al., 2017; Sigurdsson, 2016). Furthermore, we presented a *cognitive factor* uncorrelated with the latter but also impaired after ELS. This lack of association between psychotic-like behaviors and cognitive impairments suggests two neurobiological substrates, which are confirmed by our multivariate analysis, indicating the association of LTP to cognitive deficits and neuroinflammation to sensorimotor alterations.

Surprisingly, we found that cognitive impairment was associated with an abnormally increased susceptibility of HPC-PFC circuits to undergo LTP. This appears to be in contrast with previous studies, which reported reduced hippocampal LTP and cognitive deficits after ELS (Chang et al., 2003; O'Leary et al., 2016). However, no hyperexcitability or spontaneous seizures were described in these studies (O'Leary et al., 2016). In turn, Notenboom et al. (2010) used an animal model of febrile ELS and demonstrated increased LTP in HPC slices related to the reduction of seizure threshold, hyperexcitability, and spontaneous seizures later in life (i.e., epileptogenesis) (Dubé et al., 2006; Dubé et al., 2000). Indeed, paroxysmal activity had been shown to acutely increase synaptic efficacy

835 and hippocampal LTP, thereby reducing the threshold for seizure induction (Ben-
836 Ari and Gho, 1988; Minamiura A' et al., 1996). In this context, the enhanced LTP
837 observed in our data indicates a relationship with epileptogenesis, which concurs
838 with the epileptiform discharges we observed in ELS rats and the increases we
839 observed in the hippocampal Glu/GABA ratio.

840 We describe an inverted-U relationship between LTP and working
841 memory, suggesting an optimal level of LTP susceptibility is required for
842 adequate working memory performance. Aberrant synaptic plasticity could be a
843 common mechanism between cognitive deficits and epileptogenesis.
844 Hyperexcitable HPC-PFC circuits could facilitate the spread of epileptiform
845 activity and promote alterations in synaptic saturation and excitatory/inhibitory
846 balance, ultimately leading to cognitive deficits. In this sense, the abnormally
847 increased LTP could impair sensory processes during working memory and
848 explain the poor performance we observed in ELS rats. In a neural network with
849 aberrantly enhanced LTP, synaptic plasticity could be biased toward potentiation,
850 resulting in a lower ability to retain information or adapt to the environment
851 (Navakkode et al., 2022). This rationale is supported by several genetic studies,
852 including on risk genes for neuropsychiatric disorders, that described
853 relationships between enhanced LTP and impaired learning (Garcia-Alvarez et
854 al., 2015; Meng et al., 2002; Nuytens et al., 2013; Yokoi et al., 2015). Additionally,
855 enhanced HPC-PFC LTP is found in the methylazoxymethanol acetate (MAM)
856 neurodevelopmental model of schizophrenia, which also presents impaired
857 spatial working memory, reduced PPI, hypersensitivity to psychostimulants, and
858 increased DA neurotransmission (Goto and Grace, 2006). Modulation of the
859 dopaminergic system attenuated the MAM-enhanced LTP, indicating that altered
860 DA neurotransmission could underlie the LTP abnormalities in ELS rats.

861 We also report an increase in GFAP expression in ELS animals.
862 Inflammatory processes initiated by a brain insult could lead to functional
863 impairments and ultimately psychiatric symptoms (Vezzani et al., 2013). In ELS
864 models, long-term glial activation has been related to behavioral impairments and
865 epileptogenesis (de Oliveira et al., 2008), while treatment with inflammatory
866 inhibitors resulted in reductions of GFAP and cognitive impairments (Abraham et
867 al., 2012; Somera-Molina et al., 2007). High levels of pro-inflammatory
868 substances and neuroinflammation have been documented in both patients with

schizophrenia and animal models (Vezzani et al., 2013). Noteworthy, the HPC of patients with TLE and interictal psychosis present greater GFAP and microglia activation compared to TLE patients with or without depression (Kandratavicius et al., 2015). These findings are in accordance with our analysis describing enhanced GFAP as significantly contributing to psychotic-like behavioral alterations in ELS animals.

In adult SE studies, behavioral abnormalities and cognitive deficits have been positively correlated to neuronal loss and spontaneous seizure frequency (Wolf et al., 2016). It is suggested that neuropsychiatric mechanisms and epileptic excitability spread progressively over time. Indeed, the behavioral impairments in ELS models tend to be more subtle than in animal models of TLE or psychosis. It is possible that the observed neuroinflammation, neuronal dynamics, and neurochemical alterations represent initial epileptogenic pathological mechanisms that could progress to spontaneous seizures, progressive neuronal loss, and more intense behavioral manifestations (Dubé et al., 2006; Kubová and Mareš, 2013).

Dysfunctional patterns of HPC-PFC oscillatory dynamics

Our results demonstrate a locomotion-unrelated increase in HPC theta power during active behavior in ELS animals. Theta oscillations underlie various cognitive processes and are believed to serve as a temporal organizer for multiple functions, such as sensorimotor integration (Buzsáki and Moser, 2013). However, increases in HPC theta power are also observed in altered psychotic-like states, such as following ketamine administration (Caixeta et al., 2013). Increases in theta power are reported in most studies in patients with schizophrenia (Newson and Thiagarajan, 2019) and have been correlated with poor cognitive performance (Curic et al., 2021). Thus, stronger HPC theta power does not necessarily reflect an optimal cognitive state. In fact, here we observed lower theta-gamma correlations in the PFC of ELS animals, suggesting a disconnection between theta power and local coordination of PFC activity. Similarly, the ketamine model of psychosis also presents disrupted gamma coordination in the PFC (Jodo et al., 2005; Lopes-Aguiar et al., 2020). In addition, we also observed a flatter PFC power spectrum in ELS animals compared to the normal tilt of CTRL, which has been discussed to indicate excitation/inhibition imbalance (Gao et al.,

903 2017). These findings occurring during active behavior could explain the
904 cognitive-behavioral alterations we observed, at least to some extent.

905 Desynchronization between limbic-frontal circuits is also reflected by
906 reduced theta coherence during REM. Genetic and neurodevelopmental models
907 of schizophrenia exhibit a decrease in HPC-PFC theta synchrony correlated with
908 poor spatial working memory performance (Sigurdsson, 2016; Sigurdsson and
909 Duvarci, 2016). We observed impaired theta coherence only during REM sleep,
910 which is the brain state with the expected higher coherence values, indicating
911 that ELS animals could not reach or maintain this connectivity at the same
912 maximum capacity as CTRL animals. The results from oscillatory dynamics in the
913 HPC-PFC circuit indicate abnormalities in the temporal organization and
914 interaction of local circuits that can contribute to behavioral alterations and
915 cognitive deficits.

916 Our results also demonstrated that during ACT behavior, frontal-limbic
917 oscillatory dynamics of ELS rats are unusually similar to REM sleep. Importantly,
918 this finding could not be explained by altered locomotion or sleep architecture.
919 This aberrant active state was more pronounced in the initial 12 h of recording,
920 corresponding to the habituation to the novel environment. Dzirasa et al. (2006)
921 found similar results when recording hyperdopaminergic mice. The authors
922 described a REM-like awake state in DAT-KO mice and wild-type mice injected
923 with amphetamine. Similar to our results, the hyperdopaminergic wake state was
924 marked by a significant increase in hippocampal theta oscillations. Additionally,
925 treatment with antipsychotics reduced these REM-like hippocampal oscillations
926 (Dzirasa et al., 2006). Our similar findings on a developmental model resulting in
927 a psychotic-like phenotype support the relevance of intraindividual REM-wake
928 similarity as a neural mechanism of psychosis. These results also advance
929 previous studies, suggesting a shared involvement of dopamine in the impaired
930 regulation of state-dependent global network dynamics in animal models of
931 psychosis and epilepsy. Also interestingly, it is speculated that REM-wake
932 similarity may represent a neural correlate of oneiric intrusion onto awake
933 consciousness (Dzirasa et al. 2006), which, in the clinical context, could underlie
934 potential phenomenological manifestations in epilepsy-comorbid psychosis.

935 Apomorphine sensitivity has been associated with reduced PPI,
936 hyperlocomotion, and increased NAc dopamine release (Ellenbroek and Cools,

2002). Corroborating our data, neonatal SE promotes amphetamine sensitization and affects both dopaminergic and glutamatergic levels in prefrontal-striatal circuits (Lin et al., 2009). These results point to enhanced dopaminergic neurotransmission as a potential mechanism underlying the functional abnormalities observed in ELS rats.

In conclusion, we describe a comprehensive set of behavioral and neurobiological alterations following ELS that represent common patterns of dysfunctional circuit dynamics between epilepsy and psychosis. A prominent theory about the pathogenesis of schizophrenia links stressful insults during development to increased HPC excitability, which would culminate in the hyperactivation of the mesolimbic system, resulting in behavioral dysfunctions (Gomes et al., 2020). Our results add depth to this theory by finding relationships among (1) epileptogenesis, (2) hyperexcitable HPC, (3) increased DA drive, (4) disrupted information flow in limbic-frontal circuits, and (5) psychosis-relevant behaviors. Given the common pathophysiological and behavioral traits linking epileptogenesis and behavioral-cognitive comorbidities, we emphasize the model's validity to investigate the neurobiological mechanisms of how an injury during development can lead to psychiatric symptoms. Our study also demonstrates the potential of a multilevel strategy combining electrophysiology, behavior, immunohistochemistry, and neurochemistry in revealing integrated multidimensional mechanisms linking epilepsy, psychosis, and cognition.

References

Abraham J, Fox PD, Condello C, Bartolini A, Koh S. 2012. Minocycline attenuates microglia activation and blocks the long-term epileptogenic effects of early-life seizures. *Neurobiol Dis* **46**:425–430. doi:10.1016/j.nbd.2012.02.006

Baram TZ, Eghbal-Ahmadi M, Bender RA. 2002. Is neuronal death required for seizure-induced epileptogenesis in the immature brain?Progress in Brain Research. Elsevier. pp. 365–375. doi:10.1016/S0079-6123(02)35033-7

Barr DJ, Levy R, Scheepers C, Tily HJ. 2013. Random effects structure for confirmatory hypothesis testing: Keep it maximal. *J Mem Lang* **68**:255–278. doi:10.1016/j.jml.2012.11.001

970 Ben-Ari Y and, Gho M. 1988. Long-lasting modification of the synaptic properties
971 of rat ca3 hippocampal neurones induced by kainic acid, Journal of
972 Physiology.

973 Bueno-Junior LS, Peixoto-Santos JE, Ruggiero RN, Ávila MAV, Marques DB,
974 Lopes-Aguiar C, Leite JP. 2018. Interaction between hippocampal-prefrontal
975 plasticity and thalamic-prefrontal activity. *Sci Rep* **8**. doi:10.1038/s41598-
976 018-19540-6

977 Bueno-Junior LS, Ruggiero RN, Rossignoli MT, del Bel EA, Leite JP, Uchitel OD.
978 2017. Acetazolamide potentiates the afferent drive to prefrontal cortex
979 in vivo. *Physiol Rep* **5**. doi:10.14814/phy2.13066

980 Buzsáki G, Moser EI. 2013. Memory, navigation and theta rhythm in the
981 hippocampal-entorhinal system. *Nat Neurosci*. doi:10.1038/nn.3304

982 Caixeta F v., Cornélio AM, Scheffer-Teixeira R, Ribeiro S, Tort ABL. 2013.
983 Ketamine alters oscillatory coupling in the hippocampus. *Sci Rep* **3**.
984 doi:10.1038/srep02348

985 Castro-Neto EF de, Cunha RH da, Silveira DX da, Yonamine M, Gouveia TLF,
986 Cavalheiro EA, Amado D, Naffah-Mazzacoratti M da G. 2013. Changes in
987 aminoacidergic and monoaminergic neurotransmission in the hippocampus
988 and amygdala of rats after ayahuasca ingestion. *World J Biol Chem* **4**:141.
989 doi:10.4331/wjbc.v4.i4.141

990 Chang Y-C, Huang A-M, Kuo Y-M, Wang S-T, Chang Y-Y, Huang C-C. 2003.
991 Febrile Seizures Impair Memory and cAMP Response-Element Binding
992 Protein Activation. Ann. Neurol. 54(6):706-18. doi: 10.1002/ana.10789.

993 Curic S, Andreou C, Nolte G, Steinmann S, Thiebes S, Polomac N, Haaf M, Rauh
994 J, Leicht G, Mulert C. 2021. Ketamine Alters Functional Gamma and Theta
995 Resting-State Connectivity in Healthy Humans: Implications for
996 Schizophrenia Treatment Targeting the Glutamate System. *Front Psychiatry*
997 **12**. doi:10.3389/fpsyt.2021.671007

998 Dalmagro CL, Velasco TR, Bianchin MM, Martins APP, Guarnieri R, Cescato MP,
999 Carlotti CG, Assirati JA, Araújo D, Santos AC, Hallak JE, Sakamoto AC.
1000 2012. Psychiatric comorbidity in refractory focal epilepsy: A study of 490
1001 patients. *Epilepsy and Behavior* **25**:593–597.
1002 doi:10.1016/j.yebeh.2012.09.026

1003 De La Fuente-Fernández R, Lim AS, Sossi V, Holden JE, Calne DB, Ruth TJ,
1004 Stoessl AJ. 2001. Apomorphine-Induced Changes in Synaptic Dopamine
1005 Levels: Positron Emission Tomography Evidence for Presynaptic Inhibition.

1006 de Oliveira DL, Fischer A, Jorge RS, da Silva MC, Leite M, Gonçalves CA,
1007 Quillfeldt JA, Souza DO, E Souza TM, Wofchuk S. 2008. Effects of early-life
1008 LiCl-Pilocarpine-induced status epilepticus on memory and anxiety in adult
1009 rats are associated with mossy fiber sprouting and elevated CSF S100B
1010 protein. *Epilepsia* **49**:842–852. doi:10.1111/j.1528-1167.2007.01484.x

1011 Donoghue T, Haller M, Peterson EJ, Varma P, Sebastian P, Gao R, Noto T, Lara
1012 AH, Wallis JD, Knight RT, Shestyuk A, Voytek B. 2020. Parameterizing neural
1013 power spectra into periodic and aperiodic components. *Nat Neurosci*
1014 **23**:1655–1665. doi:10.1038/s41593-020-00744-x

1015 Dube C, Chen K, Eghbal-Ahmadi M, Brunson K, Soltesz I, Baram TZ. 2000.
1016 Prolonged Febrile Seizures in the Immature Rat Model Enhance
1017 Hippocampal Excitability Long Term. Ann Neurol 47(3):336-44.

1018 Dubé C, Richichi C, Bender RA, Chung G, Litt B, Baram TZ. 2006. Temporal lobe
1019 epilepsy after experimental prolonged febrile seizures: Prospective analysis.
1020 *Brain* **129**:911–922. doi:10.1093/brain/awl018

1021 Dzirasa K, Ribeiro S, Costa R, Santos LM, Lin SC, Grosmark A, Sotnikova TD,
1022 Gainetdinov RR, Caron MG, Nicolelis MAL. 2006. Dopaminergic control of
1023 sleep-wake states. *Journal of Neuroscience* **26**:10577–10589.
1024 doi:10.1523/JNEUROSCI.1767-06.2006

1025 Ellenbroek BA, Cools AR. 2002. Apomorphine Susceptibility and Animal Models
1026 for Psychopathology: Genes and Environment, Behavior Genetics.

1027 Floresco SB, Seamans JK, Phillips AG. 1997. Selective Roles for Hippocampal,
1028 Prefrontal Cortical, and Ventral Striatal Circuits in Radial-Arm Maze Tasks
1029 With or Without a Delay.

1030 Gao R, Peterson EJ, Voytek B. 2017. Inferring synaptic excitation/inhibition
1031 balance from field potentials. *Neuroimage* **158**:70–78.
1032 doi:10.1016/j.neuroimage.2017.06.078

1033 Garcia-Alvarez G, Shetty MS, Lu B, Yap KAF, Oh-Hora M, Sajikumar S, Bichler
1034 Z, Fivaz M. 2015. Impaired spatial memory and enhanced long-term
1035 potentiation in mice with forebrain-specific ablation of the Stim genes. *Front*
1036 *Behav Neurosci* **9**. doi:10.3389/fnbeh.2015.00180

1037 Gervasoni D, Lin SC, Ribeiro S, Soares ES, Pantoja J, Nicolelis MAL. 2004.
1038 Global forebrain dynamics predict rat behavioral states and their transitions.
1039 *Journal of Neuroscience* **24**:11137–11147. doi:10.1523/JNEUROSCI.3524-
1040 04.2004

1041 Gomes F v., Zhu X, Grace AA. 2020. Correction: The pathophysiological impact
1042 of stress on the dopamine system is dependent on the state of the critical
1043 period of vulnerability (Molecular Psychiatry, (2020), 25, 12, (3278-3291),
1044 10.1038/s41380-019-0514-1). *Mol Psychiatry*. doi:10.1038/s41380-019-
1045 0527-9

1046 Goto Y, Grace AA. 2006. Alterations in Medial Prefrontal Cortical Activity and
1047 Plasticity in Rats with Disruption of Cortical Development. *Biol Psychiatry*
1048 **60**:1259–1267. doi:10.1016/j.biopsych.2006.05.046

1049 Holmes GL. 2016. Effect of Seizures on the Developing Brain and Cognition.
1050 *Semin Pediatr Neurol*. doi:10.1016/j.spen.2016.05.001

Jensen FE. 2011. Epilepsy as a spectrum disorder: Implications from novel clinical and basic neuroscience. *Epilepsia* **52**:1–6. doi:10.1111/j.1528-1167.2010.02904.x

Jodo E, Suzuki Y, Katayama T, Hoshino KY, Takeuchi S, Niwa SI, Kayama Y. 2005. Activation of medial prefrontal cortex by phencyclidine is mediated via a hippocampo-prefrontal pathway. *Cerebral Cortex* **15**:663–669. doi:10.1093/cercor/bhh168

Kandratavicius L, Lopes-Aguiar C, Bueno-Júnior LS, Romcy-Pereira RN, Hallak JEC, Leite JP. 2012a. Comorbidades psiquiátricas na epilepsia do lobo temporal: Possíveis relações entre desordens psicóticas e comprometimento de circuitos límbicos. *Revista Brasileira de Psiquiatria* **34**:454–466. doi:10.1016/j.rbp.2012.04.007

Kandratavicius L, Peixoto-Santos JE, Monteiro MR, Scandiuzzi RC, Carlotti CG, Assirati JA, Hallak JE, Leite JP. 2015. Mesial temporal lobe epilepsy with psychiatric comorbidities: A place for differential neuroinflammatory interplay. *J Neuroinflammation* **12**. doi:10.1186/s12974-015-0266-z

Kandratavicius L, Ruggiero RN, Hallak JE, Garcia-Cairasco N, Leite JP. 2012b. Pathophysiology of mood disorders in temporal lobe epilepsy. *Revista Brasileira de Psiquiatria* **34**:233–259. doi:10.1016/j.rbp.2012.08.003

Kubová H, Mareš P. 2013. Are morphologic and functional consequences of status epilepticus in infant rats progressive? *Neuroscience* **235**:232–249. doi:10.1016/j.neuroscience.2012.12.055

Lesting J, Daldrup T, Narayanan V, Himpe C, Seidenbecher T, Pape HC. 2013. Directional Theta Coherence in Prefrontal Cortical to Amygdalo-Hippocampal Pathways Signals Fear Extinction. *PLoS One* **8**. doi:10.1371/journal.pone.0077707

Lin TC, Huang LT, Huang YN, Chen GS, Wang JY. 2009. Neonatal status epilepticus alters prefrontal-striatal circuitry and enhances methamphetamine-induced behavioral sensitization in adolescence. *Epilepsy and Behavior* **14**:316–323. doi:10.1016/j.yebeh.2008.12.005

Lopes-Aguiar C, Ruggiero RN, Rossignoli MT, Esteves I de M, Peixoto-Santos JE, Romcy-Pereira RN, Leite JP. 2020. Long-term potentiation prevents ketamine-induced aberrant neurophysiological dynamics in the hippocampus-prefrontal cortex pathway in vivo. *Sci Rep* **10**. doi:10.1038/s41598-020-63979-5

Marques DB, Ruggiero RN, Bueno-Junior LS, Rossignoli MT, Leite JP. 2022. Prediction of Learned Resistance or Helplessness by Hippocampal-Prefrontal Cortical Network Activity during Stress. *Journal of Neuroscience* **42**:81–96. doi:10.1523/JNEUROSCI.0128-21.2021

1090 Mathern GW, Adelson D, Cahan LD, Leite JR. 2002. Hippocampal neuron
1091 damage in human epilepsy: Meyer's hypothesis revisited, Progress in Brain
1092 Research 135:237-51. doi: 10.1016/s0079-6123(02)35023-4.

1093 Meng Y, Zhang Y, Tregoubov V, Janus C, Cruz L, Jackson M, Lu W-Y,
1094 Macdonald JF, Wang JY, Falls DL, Jia Z. 2002. Abnormal Spine Morphology
1095 and Enhanced LTP in LIMK-1 Knockout Mice. Neuron. 35(1):121-33. doi:
1096 10.1016/s0896-6273(02)00758-4.

1097 Minamiura A' Y, Hirayama K, Murata R, Matsuura S. 1996. Effect of hyperthermia
1098 on hippocampal synaptic transmission and CA3 kindling in developing rats.
1099 Brain Research 732(1-2):209-14. doi: 10.1016/0006-8993(96)00522-7.

1100 Navakkode S, Zhai J, Wong YP, Li G, Soong TW. 2022. Enhanced long-term
1101 potentiation and impaired learning in mice lacking alternative exon 33 of
1102 CaV1.2 calcium channel. *Transl Psychiatry* **12**. doi:10.1038/s41398-021-
1103 01683-2

1104 Newson JJ, Thiagarajan TC. 2019. EEG Frequency Bands in Psychiatric
1105 Disorders: A Review of Resting State Studies. *Front Hum Neurosci*.
1106 doi:10.3389/fnhum.2018.00521

1107 Notenboom RGE, Ramakers GMJ, Kamal A, Spruijt BM, de Graan PNE. 2010.
1108 Long-lasting modulation of synaptic plasticity in rat hippocampus after early-
1109 life complex febrile seizures. *European Journal of Neuroscience* **32**:749–758.
1110 doi:10.1111/j.1460-9568.2010.07321.x

1111 Nuytens K, Gantois I, Stijnen P, Iscru E, Laeremans A, Serneels L, van Eylen L,
1112 Liebhaber SA, Devriendt K, Balschun D, Arckens L, Creemers JWM,
1113 D'Hooge R. 2013. Haploinsufficiency of the autism candidate gene
1114 Neurobeachin induces autism-like behaviors and affects cellular and
1115 molecular processes of synaptic plasticity in mice. *Neurobiol Dis* **51**:144–151.
1116 doi:10.1016/j.nbd.2012.11.004

1117 O'Leary H, Bernard PB, Castano AM, Benke TA. 2016. Enhanced long term
1118 potentiation and decreased AMPA receptor desensitization in the acute
1119 period following a single kainate induced early life seizure. *Neurobiol Dis*
1120 **87**:134–144. doi:10.1016/j.nbd.2015.12.005

1121 Ozaki N, Nakahara T, Miura H, Kasahara Y, Nagatsu S. 1989. Effects of
1122 Apomorphine on In Vivo Release of Dopamine and Its Metabolites in the
1123 Prefrontal Cortex and the Striaturn, Studied by a Microdialysis Method, J.
1124 Neurochem.

1125 Peixoto-Santos JE, Velasco TR, Galvis-Alonso OY, Araujo D, Kandratavicius L,
1126 Assirati JA, Carlotti CG, Scandiuzzi RC, dos Santos AC, Leite JP. 2015.
1127 Temporal lobe epilepsy patients with severe hippocampal neuron loss but
1128 normal hippocampal volume: Extracellular matrix molecules are important for
1129 the maintenance of hippocampal volume. *Epilepsia* **56**:1562–1570.
1130 doi:10.1111/epi.13082

1131 Pinheiro J, Bates D, R Core Team. 2023. nlme: Linear and Nonlinear Mixed
1132 Effects Models. R package version 3.1-162, https://CRAN.R-
1133 project.org/package=nlme.

1134 Racine RJ. 1971. Electroencephalography and Clinical Neurophysiology
1135 MODIFICATION OF SEIZURE ACTIVITY BY ELECTRICAL STIMULATION:
1136 II. MOTOR SEIZURE. *Electroencephalogr Clin Neurophysiol* **32.**:281–94.

1137 Ruggiero RN, Lopes-Aguiar C, Leite JP. 2012. Early Life Seizures and Their
1138 Long-term Impacts on Cognition: The Role of Synaptic Plasticity
1139 Dysfunctions as an Underlying Mechanism. *Journal of epilepsy and clinical*
1140 *neurophysiology (impresso)* 18(4):114-120.

1141 Ruggiero RN, Rossignoli MT, de Ross JB, Hallak JEC, Leite JP, Bueno-Junior
1142 LS. 2017. Cannabinoids and vanilloids in schizophrenia: Neurophysiological
1143 evidence and directions for basic research. *Front Pharmacol*.
1144 doi:10.3389/fphar.2017.00399

1145 Ruggiero RN, Rossignoli MT, Lopes-Aguiar C, Leite JP, Bueno-Junior LS,
1146 Romcy-Pereira RN. 2018. Lithium modulates the muscarinic facilitation of
1147 synaptic plasticity and theta-gamma coupling in the hippocampal-prefrontal
1148 pathway. *Exp Neurol* **304**:90–101. doi:10.1016/j.expneurol.2018.02.011

1149 Ruggiero RN, Rossignoli MT, Marques DB, de Sousa BM, Romcy-Pereira RN,
1150 Lopes-Aguiar C, Leite JP. 2021. Neuromodulation of Hippocampal-Prefrontal
1151 Cortical Synaptic Plasticity and Functional Connectivity: Implications for
1152 Neuropsychiatric Disorders. *Front Cell Neurosci*.
1153 doi:10.3389/fncel.2021.732360

1154 Salpekar JA, Mula M. 2019. Common psychiatric comorbidities in epilepsy: How
1155 big of a problem is it? *Epilepsy and Behavior*. doi:10.1016/j.yebeh.2018.07

1156 Siegel M, Donner TH, Engel AK. 2012. Spectral fingerprints of large-scale
1157 neuronal interactions. *Nat Rev Neurosci*. doi:10.1038/nrn3137

1158 Sigurdsson T. 2016. Neural circuit dysfunction in schizophrenia: Insights from
1159 animal models. *Neuroscience*. doi:10.1016/j.neuroscience.2015.06.059

1160 Sigurdsson T, Duvarci S. 2016. Hippocampal-prefrontal interactions in cognition,
1161 behavior and psychiatric disease. *Front Syst Neurosci*.
1162 doi:10.3389/fnsys.2015.00190

1163 Somera-Molina KC, Robin B, Somera CA, Anderson C, Stine C, Koh S, Behanna
1164 HA, van Eldik LJ, Watterson DM, Wainwright MS. 2007. Glial activation links
1165 early-life seizures and long-term neurologic dysfunction: Evidence using a
1166 small molecule inhibitor of proinflammatory cytokine upregulation. *Epilepsia*
1167 **48**:1785–1800. doi:10.1111/j.1528-1167.2007.01135.x

1168 Tsai ML, Crutchley M, Boyce R, Ma J, Boon F, Cain DP, Leung LS. 2012. Long-
1169 lasting auditory gating deficit accompanied by GABA B receptor dysfunction
1170 in the hippocampus after early-life limbic seizures in rats. *Physiol Behav*
1171 **106**:534–541. doi:10.1016/j.physbeh.2012.03.033

Turetsky BI, Calkins ME, Light GA, Olincy A, Radant AD, Swerdlow NR. 2007. Neurophysiological endophenotypes of schizophrenia: The viability of selected candidate measures. *Schizophr Bull*. doi:10.1093/schbul/sbl060

Vezzani A, Aronica E, Mazarati A, Pittman QJ. 2013. Epilepsy and brain inflammation. *Exp Neurol*. doi:10.1016/j.expneurol.2011.09.033

Wolf DC, Bueno-Júnior LS, Lopes-Aguiar C, do Val Da Silva RA, Kandratavicius L, Leite JP. 2016. The frequency of spontaneous seizures in rats correlates with alterations in sensorimotor gating, spatial working memory, and parvalbumin expression throughout limbic regions. *Neuroscience* **312**:86–98. doi:10.1016/j.neuroscience.2015.11.008

Yokoi F, Chen HX, Dang MT, Cheetham CC, Campbell SL, Roper SN, Sweatt JD, Li Y. 2015. Behavioral and electrophysiological characterization of Dyt1 heterozygous knockout mice. *PLoS One* **10**. doi:10.1371/journal.pone.0120916

Ziermans T, Schothorst P, Magnée M, van Engeland H, Kemner C. 2011. Reduced prepulse inhibition in adolescents at risk for psychosis: A 2-year follow-up study. *Journal of Psychiatry and Neuroscience* **36**:127–134. doi:10.1503/jpn.100063

Figures and Legends

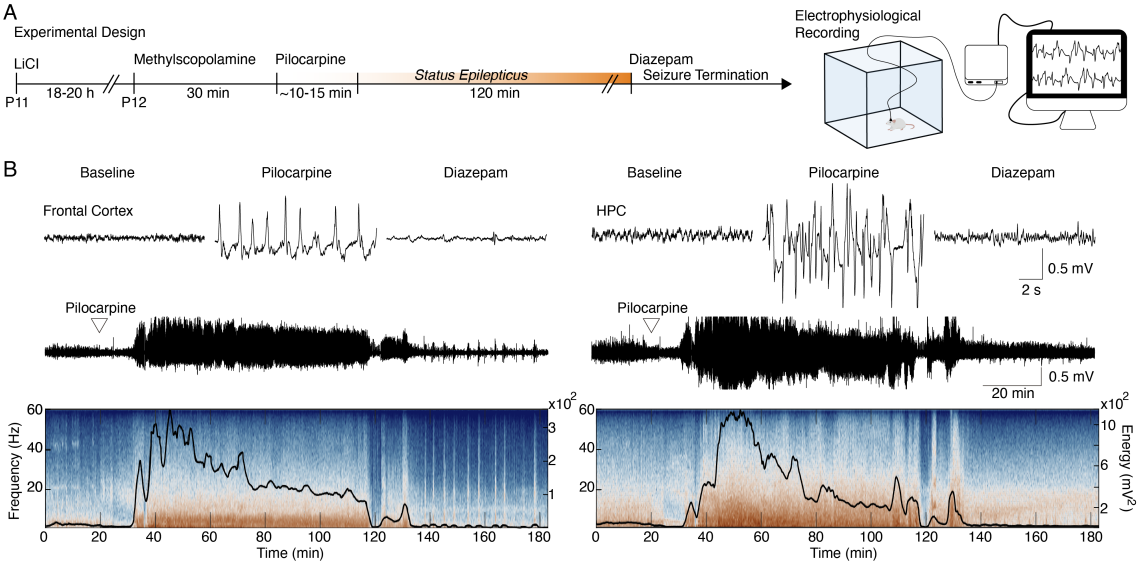

Figure 1. ELS induction. *A,* Experimental design representing early-life SE induction and monitoring. ***B,*** Representative traces of LFP during baseline, motor seizure induced by pilocarpine, and ELS interruption with diazepam injection (top). Representative LFP from the frontal cortex and HPC throughout the experiment (middle). LFPs are aligned with their respective spectrograms and energy curves (bottom).

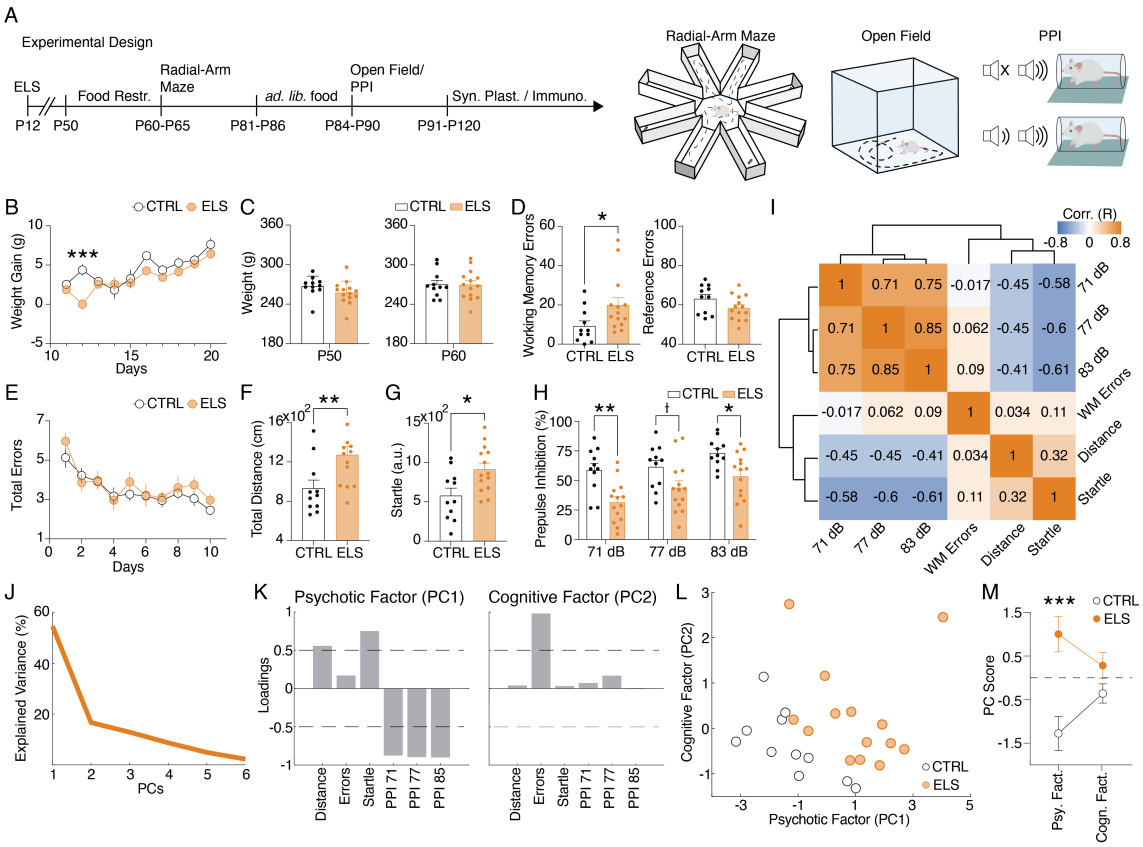

Figure 2. ELS induces a psychotic-like behavioral phenotype. *A,* Experimental design representing early-life SE induction, age of the animals during the experiments, and behavioral tests performed. ***B,*** Weight gain after ELS induction. ELS rats showed weight loss only on the ELS induction day. ***C,*** No weight differences between ELS and CTRL during experiments in adulthood, regardless if before food restriction (left) or during food restriction (right). ***D,*** Working memory task on the radial-arm maze. ELS rats showed an increase in working memory errors across sessions (left) without differences in the number of reference errors (right). E, ELS rats showed a similar learning curve when compared to CTRL. ***F,*** Hyperlocomotion of ELS rats in the open field test. ***G,*** Higher acoustic startle of ELS rats. ***H,*** Impaired sensorimotor gating in ELS rats as measured in the PPI test with three stimulus intensities. ***I,*** Correlation matrix of all behavioral variables. Note a cluster of positive correlations formed by the PPI measures and another cluster of negative correlations formed by the PPI measures with distance traveled on the open field and the acoustic startle. Working memory errors were not correlated with the other behavioral features. ***J,*** Explained variance from principal components analysis (PCA). Note that the two first PC explain 71.32% of the data. ***K,*** Loadings of the behavioral variables on each principal component (PC) reveal a *psychotic factor* (PC1) and an uncorrelated *cognitive factor* (PC2). ***L,*** PCA of the behavioral features showing each animal projected onto the new factors. ***M,*** The psychotic factor distinguishes ELS from CTRL animals, as we compare the PC scores from each group. † $p < 0.1$, *$p < 0.05$, **$p < 0.01$, ***$p < 0.001$. Error bars represent the mean ± SEM.

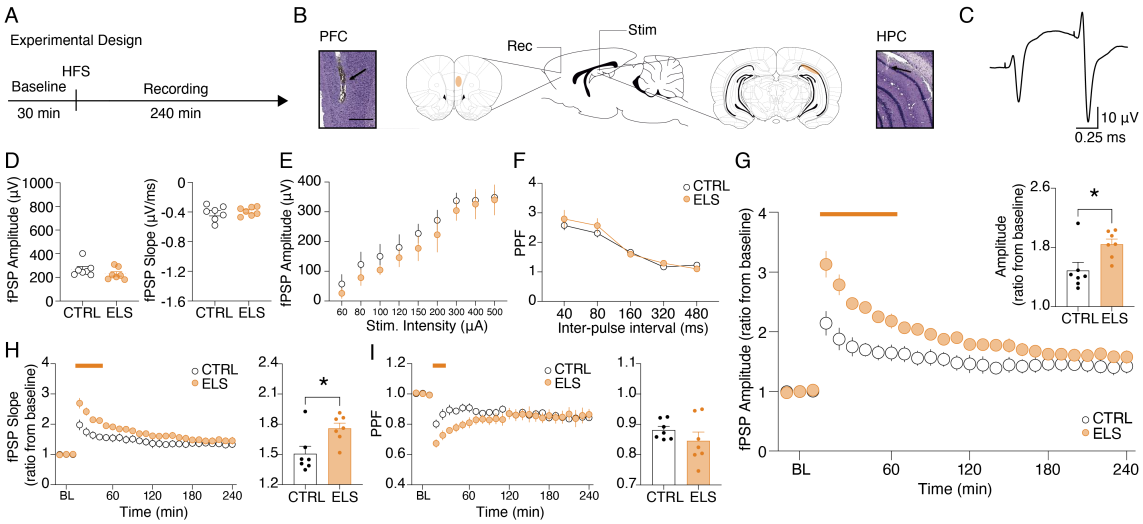

Figure 3. Aberrant HPC-PFC synaptic plasticity in animals submitted to ELS. *A,* Experimental design including high-frequency stimulation (HFS) to LTP induction. ***B,*** Electrode placement and representative electrolytic lesions in Nissl-stained coronal sections. ***C,*** Representative evoked fPSPs in the PFC. No difference between ELS and CTRL rats in terms of basal neurotransmission and synaptic efficacy, as shown by: ***(D)***, fPSP amplitude (left) and slope (right); ***(E),*** input-output curve; and ***(F),*** paired-pulse facilitation (PPF) curve. ***G,*** Despite no changes in basal synaptic efficacy, ELS rats showed aberrantly increased LTP, represented by higher fPSP amplitude ratios from baseline (BL) post-HFS, both across time blocks (main curve graph) and their averages (bar graph, inset). ***H,*** As in ***G,*** but from fPSP slopes. ***I,*** ELS rats showed reduced PPF in the initial 30 min (curve graph). Averaged data resulted in no differences between the groups (bar graph, inset). † $p < 0.1$, *$p < 0.05$, **$p < 0.01$, ***$p < 0.001$. Error bars represent the mean ± SEM.

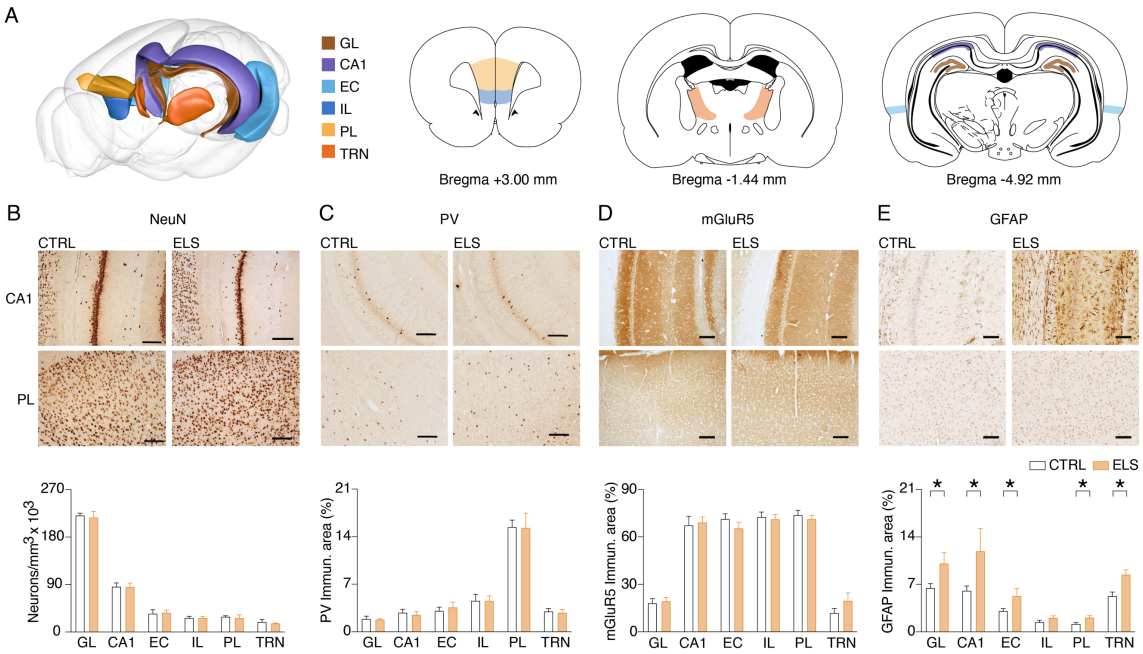

Figure 4. ELS induces long-term neural inflammation, but not neuronal loss. ***A*** 3-D brain diagram and coronal sections representing the brain regions investigated. ***B-E***, Representative photomicrographs from immunohistochemistry each pair of columns represents a group comparison (left CTRL and right ELS) and each line is related to CA1 and PL, respectively. ***B,*** NeuN immunohistochemistry showing that ELS rats did not present neuronal loss. ***C,*** Parvalbumin (PV) immunohistochemistry. ***D,*** mGluR5: ***E***, GFAP, showing increased astrogliosis induced by ELS. GL: Granule layer of dentate gyrus; CA1: *Cornu Ammonis* 1; EC: Entorhinal cortex; IL: Infralimbic cortex; PL: Prelimbic cortex; TRN: Thalamic Reticular Nucleus. *$p < 0.05$ Error bars represent the mean ± SEM.

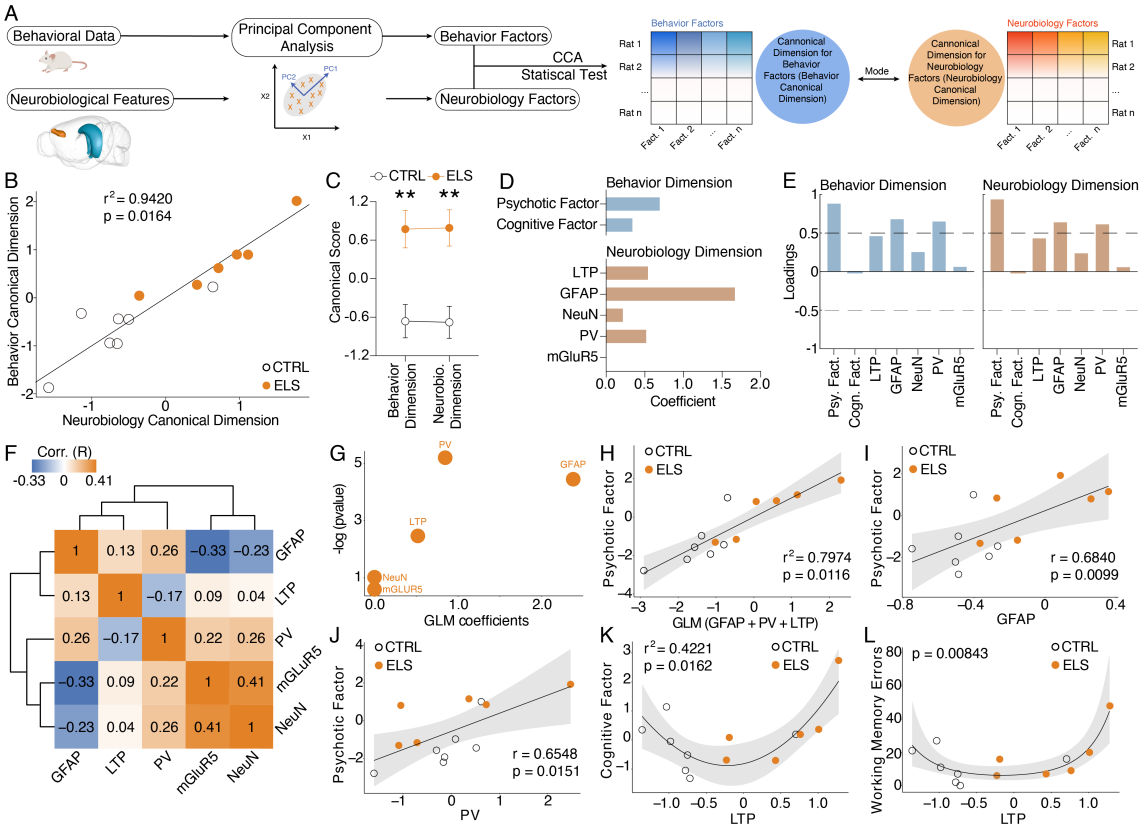

Figure 5. Cognitive impairment and psychotic-like behavior are distinctly correlated with abnormal LTP and neuroinflammation. *A,* Steps performed in data processing and analysis for canonical correlation analysis (CCA). ***B,*** CCA analysis showing CTRL and ELS animals projected onto the first canonical correlation. We found a strong correlation between the neurobiology canonical dimension and the behavior canonical dimension. ***C,*** Canonical scores showing the clear CTRL *vs.* ELS difference that the CCA was able to capture. ***D,*** Coefficients for behavior and neurobiology canonical dimensions, showing greater contributions of the psychotic factor, GFAP, PV, and LTP for the correlation. ***E,*** Loadings of the behavioral and neurobiological variables on each canonical correlation dimension indicating an association between GFAP and PV with the psychotic behavioral factor. ***F,*** Correlation matrix showing only weak correlations between the neurobiological features. ***G,*** GLM regression between neurobiological features and the psychotic factor. ***H***, GLM model between neurobiological features and the psychotic factor show a strong association with GFAP, PV, and LTP. ***I,*** GLM regression between LTP and the cognitive factor shows a quadratic association (left). This quadratic association was further confirmed performing a quasi-Poisson regression between LTP and raw values of working memory errors (right). **p < 0.01. Error bars represent the mean ± SEM.

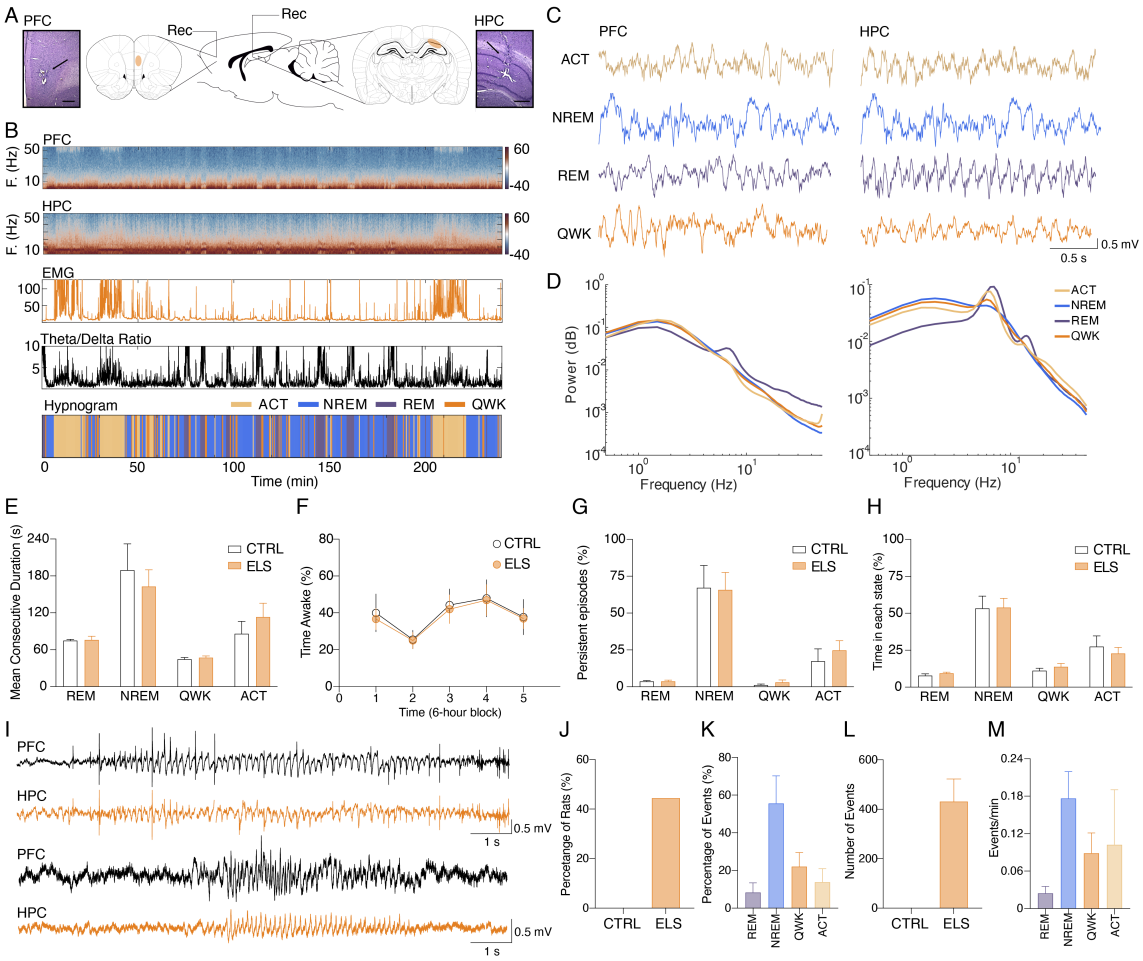

Figure 6. Classification of sleep-wake states and electrographic discharges in ELS rats. *A,* Electrode placement and representative electrolytic lesions in Nissl-stained coronal sections. ***B,*** Representative spectrogram, electromyogram (EMG) root mean squared (RMS), and HPC theta/delta ratio used to score the sleep-wake cycle and to generate the hypnogram (bottom). ***C,*** Representative LFPs (top) recorded from PFC and HPC during ACT, NREM, REM, and QWK. ***D,*** Average power spectral density for each state in the PFC and HPC of a representative CTRL animal. Note the increase in HPC theta power during ACT and REM. ELS rats did not present alterations in the sleep-wake cycle. ***E-G***, There were no differences between ELS and CTRL in the ***(E)*** Mean duration of consecutive epochs for each state, ***(F)*** percentage of time awake across 6-h blocks, and in the ***(G)*** number of persistent episodes (episodes lasting longer than 3 s, top) or the percentage of time spent in each state (bottom). ***H,*** Representative LFP from PFC and HPC showing a representative spike-wave discharge (SWD, top) and a poly-spike discharge (bottom). ***I,*** Representative LFPs with clear electrographic discharges of two ELS rats (top and bottom). Electrographic discharges were found in 44.5% of ELS animals and were absent in CTRL animals. ***J,*** Percentage of events occurring in each sleep-wake stage. ***K,*** Average total number of SWD events in CTRL and ELS animals. ***L,*** Frequency of SWDs occurring per state. SWDs events rarely occurred during REM. Error bars represent the mean ± SEM.

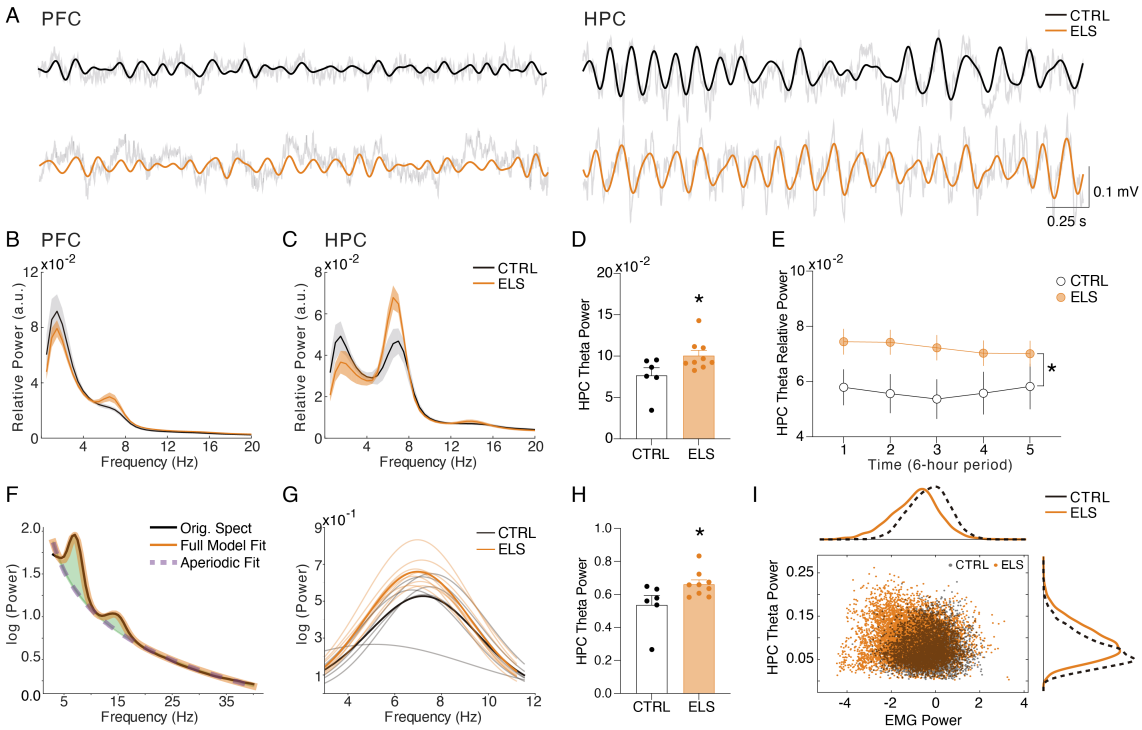

Figure 7. Increased HPC theta power during behavioral activity in ELS animals. *A,* Representative raw LFPs (transparent black lines) and theta-filtered signal of CTRL (black) and ELS (orange) from the PFC (left) and HPC (right) during ACT. ***B,*** Relative PSD of the PFC during ACT. ***C,*** Relative PSD of the HPC during ACT. ***D,*** ELS rats present an enhanced HPC theta power during ACT. ***E,*** Theta relative power during each of the 6-hour periods of recording, showing a general increase in the ELS animals that is more pronounced in the initial 18 h of recording. ***F,*** Parametric model used to distinguish oscillatory from aperiodic component. ***G,*** Oscillatory components extracted from ACT PSDs used to calculate theta power. ***H,*** Theta power increase in ELS rats is due to a true oscillatory component and not from the aperiodic activity in ACT states. ***I,*** Theta power increase in ELS rats is independent of locomotor activity. Note from the distribution of relative theta power and Z-scored EMG (trapezius) values for all rats that EMG power is not related to the regions of greater theta power in the ELS animals. *$p < 0.05$. Error bars represent the mean ± SEM.

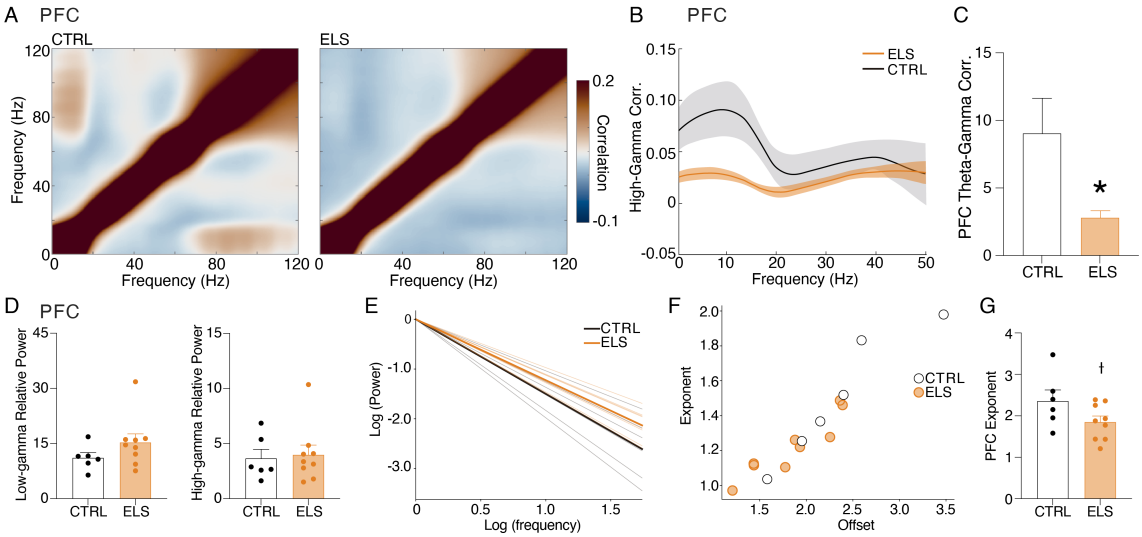

Figure 8. ELS promotes abnormal gamma coordination in the PFC during behavioral activity. ELS rats present an abnormal gamma activity in the PFC. ***A,*** Grand-average amplitude correlogram for CTRL (left) and ELS (right) group. Note the absence of amplitude correlation between theta and gamma activity in the ELS group. ***B,*** High-gamma (65-100 Hz) correlation with low-frequency activity. Note the peak around theta oscillation in the CTRL group and the absence in ELS. ***C,*** ELS present an impaired theta-gamma amplitude correlation. ***D,*** There is no difference between the low- (top) and high-gamma (bottom) average power. ***E,*** Aperiodic activity extracted from the PFC of each rat during ACT state. ***F,*** Distribution of the parameters of the aperiodic component (exponent and offset) for each rat. ***G,*** ELS rats show a tendency to reduction (p = 0.0656) in the exponent parameter of the aperiodic component. † $p < 0.1$, *$p < 0.05$. Error bars represent the mean ± SEM.

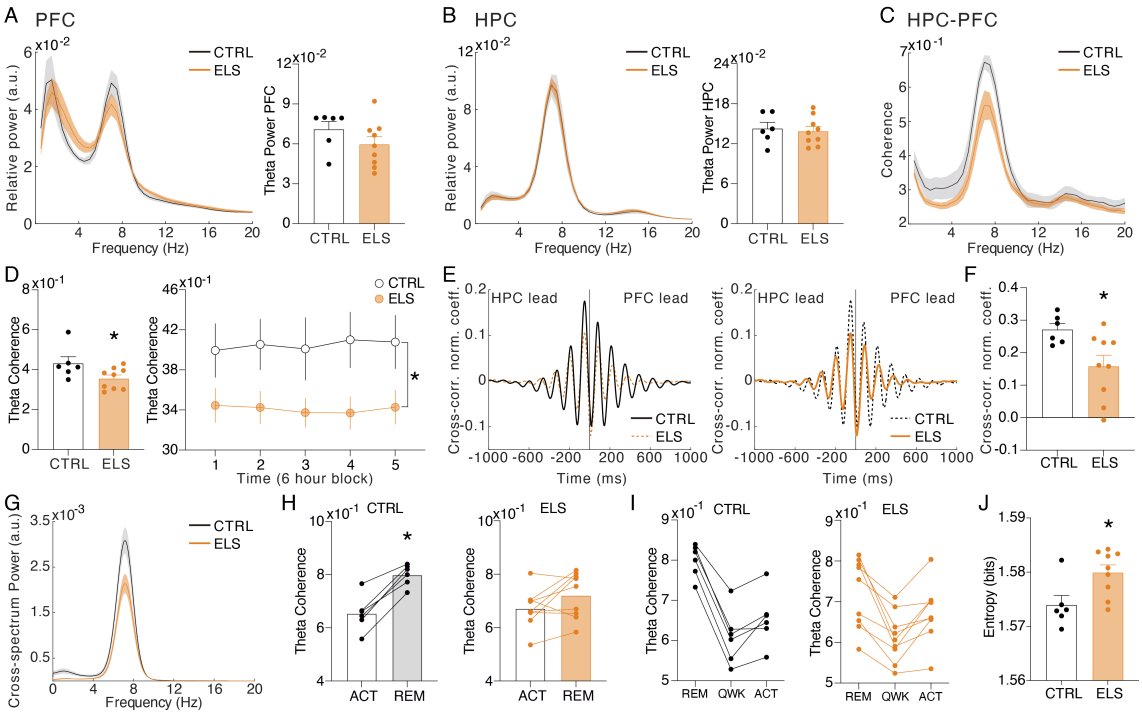

Figure 9. ELS impairs HPC-PFC coherence during REM sleep. *A,* PSD in the PFC during REM. ***B,*** PSD in the HPC during REM. No significant alterations in theta power during REM are observed in ELS rats. ***C,*** Theta coherence is diminished in ELS rats. ***D,*** Significant effect on the HPC-PFC theta coherence by averaging the entire recording (left) and across all periods (right). ***E,*** Time domain cross-correlation between PFC and HPC LFPs during REM epochs highlighting CTRL (left) and ELS (right) group averages. ***F,*** Reduction in the peak of correlation between -80 to -20 ms in ELS rats***. G,*** Average cross-spectrum power density showing a reduced theta peak in the ELS rats. ***H,*** Theta HPC-PFC coherence increases from ACT to REM states. We can observe that all the CTRL rats present an increase from ACT to REM, while in ELS rats this is not observed. Paired *t*-test *p < 0.05. ***I,*** Theta coherence dynamics across the sleep-wake cycle. CTRL rats display a homogeneous dynamics with theta coherence being maximal at REM, minimal in QWK, and intermediate in ACT states. This dynamics is disrupted in ELS rats that display a higher variance between animals, with some animals displaying similar coherence in REM and ACT. ***J,*** Entropy of the theta coherence dynamics is higher in ELS rats, representing the more homogeneous values across states.

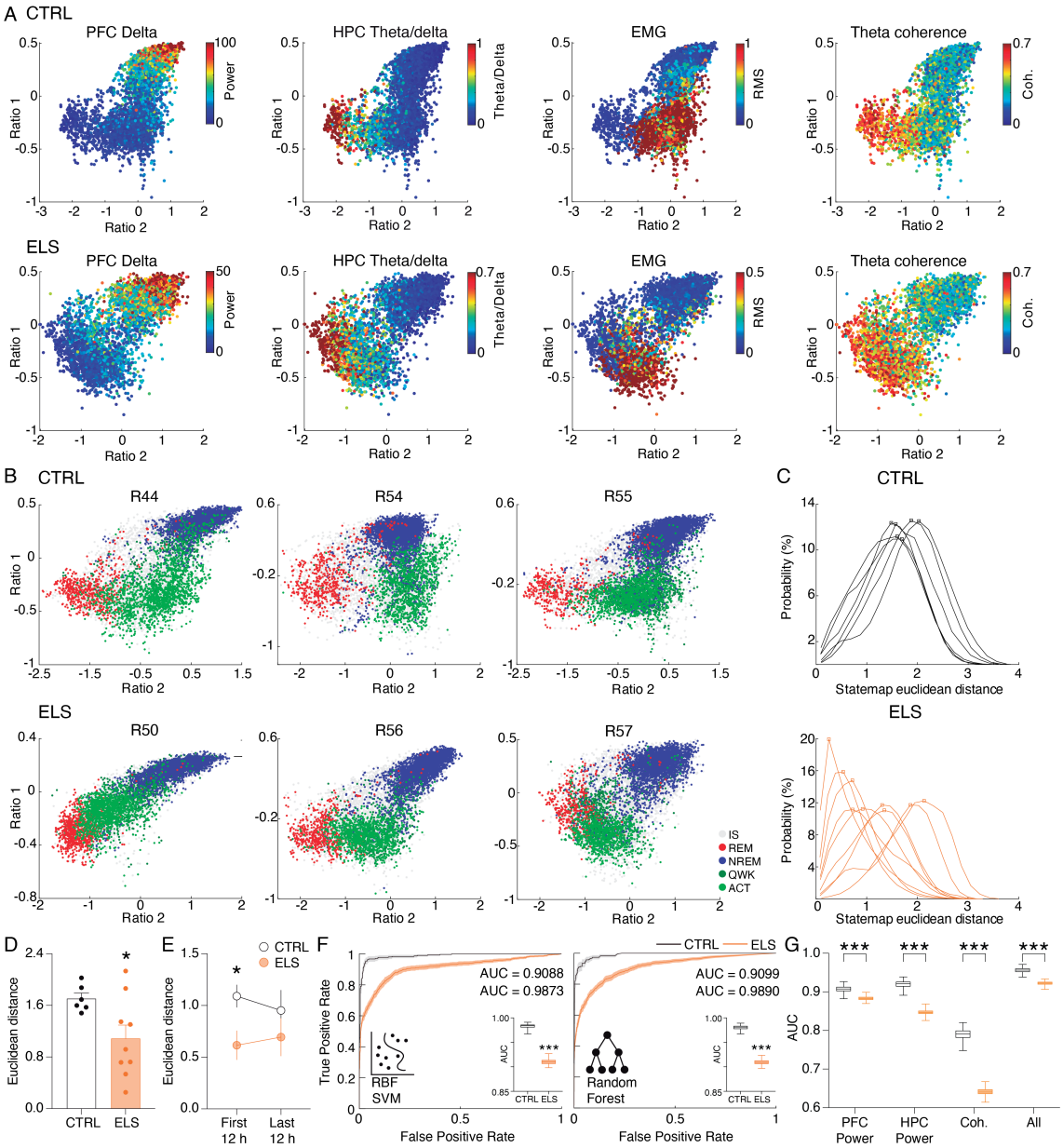

Figure 10. ELS rats display REM-like oscillatory dynamics during active behavior. *A,* State map construction reflects the sleep-wake cycle and spectral dynamics for one representative CTRL (top) and ELS (bottom) rat. PFC delta power is evident during NREM, theta/delta ratio is maximum in REM, EMG power describes ACT states, and HPC-PFC theta coherence is stronger close to REM. Note that in the ELS rat, the coherence is also broadly high during the ACT state. ***B,*** Representative state maps from three CTRL (top) and three ELS (bottom) rats. CTRL rats displayed a clear separation between REM (red), ACT (light green), and NREM (blue) clusters. ELS displayed an overlap between REM and ACT states. ***C,*** Distributions of the Euclidean distances between each REM and ACT epoch for CTRL (top) and ELS (bottom) rats. ELS distributions were heterogeneous, some of which were skewed. ***D,*** Average Euclidean distance showing that ELS rats have REM-like oscillatory dynamics during active behavior. ***E,*** REM-like oscillations during ACT were more pronounced in ELS during the initial 12 h of recording. ***F,*** Machine learning approach to decode REM *versus* ACT states. We used radial basis function

support vector machine (SVM) and random forest (RF) algorithm in order to classify REM and ACT epochs in CTRL (black) or ELS (orange) rats. Using a bootstrapped confidence interval, we observed that the discriminative performance was worse in ELS animals, even when using “brute-force” algorithms. ***G,*** A machine learning algorithm (random forest) fitted on whole-spectrum data also shows a significantly worse performance in ELS for PFC power, HPC power, coherence, and all estimates combined. † $p < 0.1$, *$p < 0.05$, **$p < 0.01$, ***$p < 0.001$. Error bars represent the mean ± SEM.

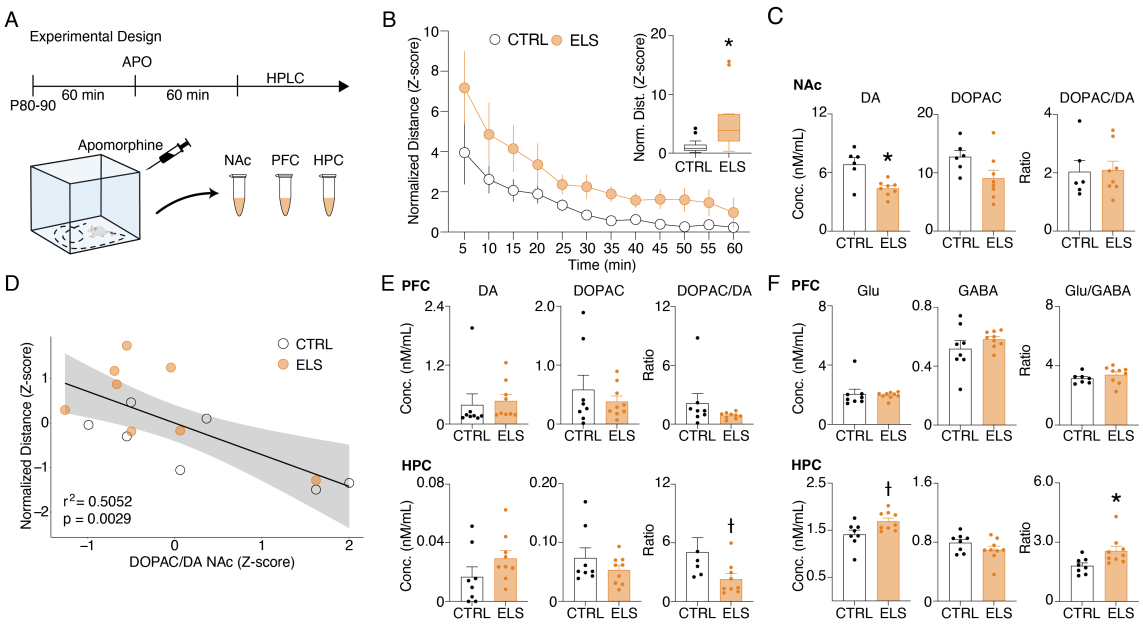

Figure 11. ELS rats present behavioral and neurochemical sensitivity to dopaminergic activation. *A,* Experimental design representing quantification of locomotion in the open field, apomorphine (APO) injection, and neurochemical analysis. ***B,*** Normalized locomotion across time blocks after APO injection, demonstrating increased locomotion of ELS rats induced by APO. Average normalized locomotion after APO injection (inset). ***C,*** Concentration of dopamine and metabolites in the NAc. ***D,*** GLM for the total distance after APO indicating DOPAC/DA ratio in the NAc as a strong significant variable associated with behavioral sensitivity to APO. ***E,*** Concentration of dopamine and metabolites (left) in the PFC (upper panel) and HPC (lower panel). Concentration of glutamate and GABA (right) in the PFC (upper panel) and HPC (lower panel). †Uncorrected $p < 0.05$, * multiple comparison corrected $p < 0.05$. Error bars represent the mean ± SEM.

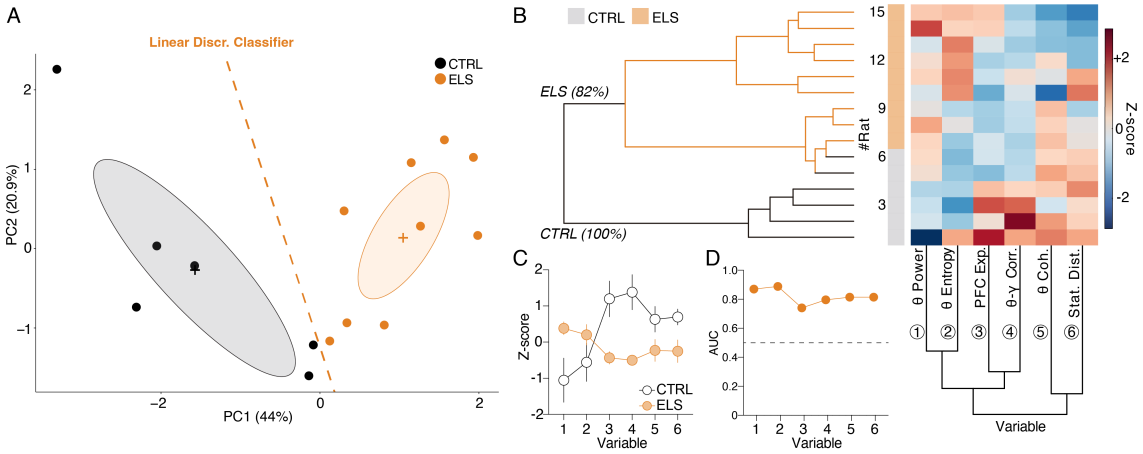

Figure 12. HPC and PFC oscillatory dynamics discriminate ELS rats. *A,* A linear discriminant classifier (dotted orange line) using the first two principal components (PCs) of relevant electrophysiological variables completely distinguishes ELS from CTRL rats (100% accuracy; 93.34% leave-one-out cross-validation). Note that the PC1 alone completely discriminates ELS rats. ***B,*** Unsupervised hierarchical clustering using the electrophysiological variables (bottom dendrogram) almost completely dissociates ELS from CTRL rats (left dendrogram). Inside the ELS cluster, we can observe one complete ELS branch, but the other overlapping with some CTRL animals, suggesting a graduality in the pathophysiological effects of ELS. ***C,*** Cluster centroids of the ELS and CTRL clusters showing distinct patterns of activity for each cluster. ***D,*** All the electrophysiological variables are good discriminators of CTRL and ELS rats (AUC-ROC > 0.7). † $p < 0.1$, *$p < 0.05$, **$p < 0.01$, ***$p < 0.001$. Error bars represent the mean ± SEM.